

Do assumptions about the central density of subhaloes affect dark matter annihilation and lensing calculations?

Nicole E. Drakos,^a James E. Taylor,^{b,c} and Andrew J. Benson^d

^aDepartment of Physics and Astronomy, University of Hawaii,
Hilo, 200 W Kawili St, Hilo, HI 96720, USA

^bDepartment of Physics and Astronomy, University of Waterloo,
200 University Avenue West, Waterloo, ON N2L 3G1, Canada

^cWaterloo Centre for Astrophysics, University of Waterloo,
200 University Avenue West, Waterloo, ON N2L 3G1, Canada

^dCarnegie Observatories,
813 Santa Barbara Street, Pasadena, CA 91101, USA

E-mail: ndrakos@hawaii.edu, taylor@uwaterloo.ca, abenson@carnegiescience.edu

Abstract. A growing body of evidence suggests that the central density of cuspy dark matter subhaloes is conserved in minor mergers. In contrast to this, empirical models of subhalo evolution, calibrated using limited-resolution simulations, often assume a drop in the central density. These empirical models are an important component in galaxy-galaxy lensing studies and dark matter annihilation calculations. We explore the dependence of these calculations on the assumed subhalo properties. We find that annihilation calculations are very sensitive to the assumed inner density profile, and different models can produce more than an order of magnitude difference in the J -factor and boost factor in individual haloes, and a factor of ~ 5 in the total annihilation rate expected in the halo Milky Way. Since the innermost parts of haloes will always be difficult to resolve in simulations, we conclude that it is important to develop a theoretical understanding of subhalo evolution to be able to make accurate predictions of the dark matter annihilation signal. On the other hand, while the shear and convergence profiles used in galaxy-galaxy lensing are sensitive to the initial profile assumed (e.g., NFW versus Einasto), they are otherwise well-approximated by a simple stripping model in which the original profile is sharply truncated at a tidal radius.

Keywords: dark matter theory, semi-analytic modeling, gamma ray theory

¹Corresponding author.

Contents

1	Introduction	1
2	Halo Models	2
2.1	Isolated dark matter haloes	2
2.2	Tidally-stripped dark matter subhaloes	3
2.3	This work	4
3	Evolution of the concentration parameter	6
4	Dark matter annihilation	10
4.1	Boost Factor Evolution	11
4.2	J -Factor Evolution	13
4.3	Dependence on structural parameters	15
4.4	Model Sensitivity in Annihilation: Summary	16
4.5	Implications for the Milky Way	17
5	Lensing	19
5.1	Model Comparisons	20
5.2	Model Sensitivity in Lensing: Summary	23
6	Discussion	24
7	Conclusion	25

1 Introduction

Dark matter haloes grow through repeated, hierarchical mergers, and simulations of this process predict that the central regions of merging haloes can survive as self-bound substructures within the final system. These ‘subhaloes’ should host most of the visible galaxies in the low-redshift Universe, and may be one of the best environments in which to explore and constrain the particle nature and non-gravitational properties of dark matter [see e.g. 7, for a review].

In general, observational tests of this predicted dark matter distribution include galaxy dynamics, gravitational lensing, and ‘indirect detection’ (i.e., searches for radiation or products from dark matter annihilation). All of these tests are most sensitive where dark matter densities are highest, at small radii within haloes and subhaloes. The annihilation signal in particular will depend sensitively on subhalo density profiles, concentration, mass loss, and disruption [as summarized in, e.g. 1, 68]. Since this signal is proportional to the local density squared, one must understand the details of the density distribution within haloes and subhaloes, down to the smallest scales on which CDM can cluster, to place reliable constraints on dark matter particle properties.

The visible structure of galaxies can be used to trace the central density distribution in haloes [e.g. 81, and references therein], but only out to a few percent of the virial radius [53, 75]. Typically, measurements of the inner core or cusp of dwarf-galaxy haloes require tens of thousands of stars and are sensitive to dynamical assumptions [9]. Gravitational lensing studies can probe the total mass distributions around galaxies, groups, and clusters more

directly. However, while gravitational lensing has the advantage of being insensitive to the dynamical state of the system, the effect is normally weak enough that good models of the lens potential are required. As first shown by [61] and since measured in several studies [e.g. 30, 54, 56, 65, 74, 85], the tidal truncation of galaxy haloes within clusters relative to those of field galaxies is detectable in lensing and needs to be included in models of the total mass distribution to obtain accurate halo mass estimates [3].

As subhaloes orbit within a larger system post-merger, they will lose mass through tidal stripping. This process generally works from the outside in [e.g. 23, 39]. However, the exact effect of tidal stripping in the innermost part of the subhalo remained unclear from previous work, given the resolution limits of simulations. In principle, repeated mass loss can also disrupt substructure completely, as is often seen in cosmological simulations of halo formation. Recent work suggests that much of this disruption is artificial, and due to insufficient resolution [5, 82, 83], and that the central density of cuspy subhaloes should be preserved to arbitrarily small masses [27, 33, 50].

Fundamentally, subhalo structure depends on the initial properties of the halo at infall and the subsequent effect of tidal evolution. Studies of the earliest forming haloes—which are expected to exist as subhaloes at low redshifts—suggest that these objects are cuspier than systems that form later, and have an inner density profile of the form $r^{-1.5}$ [e.g. 2, 15, 19, 45, 67]¹ Given the strong dependence of the annihilation signal on the dark matter density on the smallest scales and in the densest systems, this has enormous implications for current annihilation constraints [16]. For instance, it has been suggested that there should be $\sim 10^{16}$ “prompt cusps” in the Milky Way [18], which would contribute 20-80 per cent of a putative annihilation γ -ray background [79].

The current study aims to consider how modelling assumptions for subhalo density profiles affect the dark matter annihilation and lensing signals in individual subhaloes. The structure of this paper is as follows: first, in Section 2, we summarize the subhalo models considered in this work. In Section 3, we show how the concentration evolves in these different models. In Sections 4 and 5, we explore the implications of a conserved central density to the dark matter annihilation rate and lensing signal, respectively. Finally, we discuss our results in Section 6 and conclude in Section 7.

2 Halo Models

2.1 Isolated dark matter haloes

Most of our understanding of halo structure comes from cosmological simulations. One of the most important results from these studies is that isolated haloes have a universal density profile (UDP) when averaged spherically. The UDP was originally approximated in [62, 63]—hereafter NFW—as:

$$\rho_{NFW}(r) = \frac{\rho_0 r_s^3}{r(r+r_s)^2} \ , \quad (2.1)$$

where ρ_0 is a characteristic density and r_s is the scale radius, describing the point where the logarithmic slope is $d \log \rho / d \log r = -2$.

¹This is steeper than the commonly-used NFW profile, which has an inner density profile of r^{-1} , as discussed in Section 2.1.

Though NFW profiles are still commonly assumed in cosmological calculations, dark matter haloes in cosmological simulations are better described by an Einasto profile [32]

$$\rho_{Ein}(r) = \rho_{-2} \exp\left(-\frac{2}{\alpha} \left[\left(\frac{r}{r_{-2}}\right)^\alpha - 1\right]\right), \quad (2.2)$$

where ρ_{-2} and r_{-2} correspond to where the logarithmic slope is $d \log \rho / d \log r = -2$. This fit provides a better description of the UDP down to the resolution limit of simulations [35, 52, 64]; the detailed form of the profile at very small radii remains uncertain.

The ‘‘shape’’ parameter, α , controls the inner slope of the density profile, with small α values corresponding to ‘‘cuspiers’’ centres. The mean value of α increases with peak height within the cosmological density field [35, 52]; for low peaks (i.e. low-mass and/or low redshift haloes) with values of $\alpha \sim 0.2$ – 0.25 , the Einasto profile is very similar to the NFW profile, while for rare, recently-formed and/or high-mass objects, it is smoother with a shallower inner slope.

Aside from their density profiles, haloes are often described by their mass and concentration. The concentration parameter c is usually defined as the ratio of the virial radius to the scale radius, or more generally, the radius at which the logarithmic density profile has a slope of -2 , i.e., $c = r_{\text{vir}}/r_{-2}$ [63]. Concentration is broadly correlated with formation epoch, early-forming haloes being more concentrated, though the details of the relationship are complicated [e.g. 11, 58, 86, 87, 89, 91, 92].

2.2 Tidally-stripped dark matter subhaloes

As haloes merge hierarchically, tidal stripping primarily removes material from the outer radii, causing characteristic changes to the density profile. These tidally stripped systems are often described by empirical models calibrated to simulations. The first of these models was developed in [39]—hereafter H03—which posits that at large radii, the slope of tidally stripped systems is $d \log \rho / d \log r = -4$, and the central density is decreased, according to the parameterized equation:

$$\rho(r) = \frac{f_t}{1 + (r/r_{te})^3} \rho_{NFW}(r). \quad (2.3)$$

where r_{te} is an ‘‘effective’’ tidal radius, and f_t describes the reduction in central density. Both of these parameters can be estimated using a single parameter—the bound mass fraction, f_b , of the satellite:

$$\begin{aligned} \log(r_{te}/r_s) &= 1.02 + 1.38 \log f_b + 0.37(\log f_b)^2 \\ \log f_t &= -0.007 + 0.35 \log f_b \\ &\quad + 0.39(\log f_b)^2 + 0.23(\log f_b)^3. \end{aligned} \quad (2.4)$$

In H03, the bound mass fraction f_b is defined as the mass of the bound satellite compared to the mass of an untruncated NFW profile within radius $r_{\text{vir}} = 10$.

The disadvantage of empirical methods like H03 is that these models are only valid across the range of models considered in the simulations, and therefore are generally limited to specific density profiles and orbital parameters. Additionally, these models may include numerical artefacts. For example, H03 predicts an artificial reduction in the central density due to the approximation they used to set up the initial conditions in their simulations [49]. More recent empirical models [e.g. 36, 69] predict similar trends but with less reduction in the central density. In general, empirical models accurately reproduce a suite of isolated

simulation results by construction, but cannot be reliably extrapolated beyond the suite of simulations. Since the very centre of haloes will never be satisfactorily resolved in N -body simulations due to two-body interactions, these parameterizations are not able to predict the evolution at small radii/small mass fractions [27].

An alternative approach is to model the evolution of subhaloes using physical principles. This approach is generally less accurate than calibrated empirical models, with the possible exception being the Energy Truncation model developed in [25, 26] [see also 88]. The Energy Truncation model is based on the observation that particles are primarily stripped as a function of their energy [e.g. 10, 25, 78]. In practice, this energy truncation is performed by lowering and shifting the distribution function, f_0 , of the initial profile, according to

$$f(\mathcal{E}) = f_0(\mathcal{E} + \mathcal{E}_T) - f_0(\mathcal{E}_T) , \quad (2.5)$$

where $\mathcal{E} = \Psi(r) - v^2/2$ is the relative “binding” energy and $\Psi(r) = -\phi(r)$ is the relative potential energy. The parameter \mathcal{E}_T is termed the truncation energy and sets the mass and tidal radius of the truncated system. Then, the potential of this system can be found by solving Poisson’s equation and Eddington’s inversion of the density profile [31]. This procedure is analogous to the derivation of the King model [51] and has been described in detail in [25–27]. The free parameter \mathcal{E}_T can be determined from the orbital parameters of the merger [26], and thus, the Energy Truncation model has no free parameters (i.e., it does not need to be tuned to simulations).

Figure 1 demonstrates how well the Energy Truncation model predicts the subhalo density profile evolution compared to empirical models calibrated to match simulations [36, 39, 69]. We have used two simulations; Example 1 is demonstrative of a case in which the Energy Truncation Model works quite well, and Example 2 is a case where the Energy Truncation Model does not work as well; these correspond to the Slow and Fast Mass loss simulations in [27]. In general, the Energy Truncation model predicts a higher central density than the other models, and the [39] model (H03) predicts the lowest central density.

Overall, the Energy Truncation model agrees very well with isolated simulations and has comparable accuracy to parameterized models above within the range of radii that is properly resolved in simulations [26]. Further, the Energy Truncation model appears to be universally applicable to any tidally-stripped collisionless system [27]. Unlike most empirical parameterizations, the Energy Truncation model predicts the central density is preserved, which may have important consequences for applications such as dark matter annihilation and lensing predictions.

2.3 This work

Overall there is some fundamental uncertainty in the original density profile of isolated haloes (e.g. NFW and the range of Einasto profiles) and the way they are modified by tidal stripping. It is impossible to completely resolve these uncertainties by direct numerical simulation: given the limited dynamic range of simulations, we will never be able to resolve the very centre of haloes. As a result, the central density of subhaloes may be higher than previously expected. In the remaining sections of the paper, we examine how this influences the dark matter annihilation and galaxy lensing signals.

We will consider three initial profiles

1. an NFW profile, for comparison with previous work
2. a more “cuspy” Einasto profile (EinLow; $\alpha = 0.15$), and

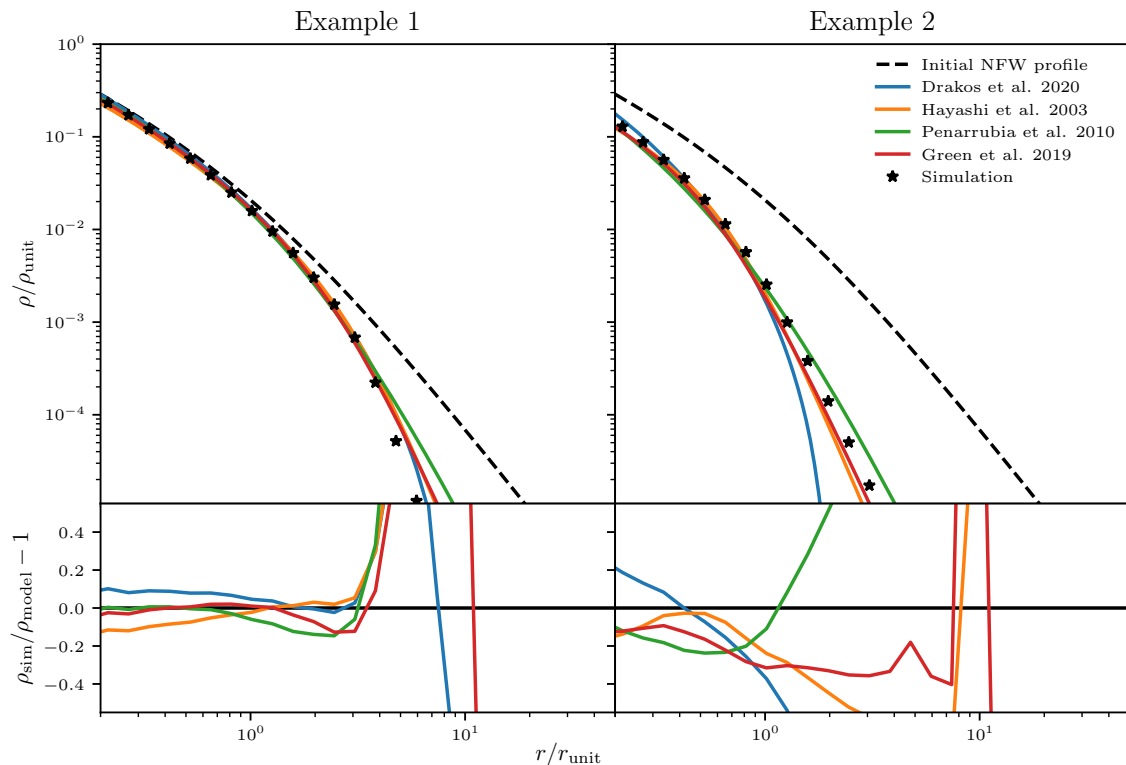


Figure 1. Comparison of models for tidally stripped NFW haloes. The simulation results are from an idealized simulation of an NFW subhalo inside a fixed background potential after 5 orbits. Examples 1 and 2 correspond to the Slow and Fast Mass loss simulations in [27]. The Energy Truncation Model [26] has no free parameters, while the three parametric models [36, 39, 69] are calculated from the bound mass of the simulated subhalo. Overall, all of the models do a comparable job of predicting the subhalo density profile.

3. a more “cored” Einasto profile (EinHigh; $\alpha = 0.3$).

These Einasto parameters were chosen since they span the range of parameters found in simulations [e.g. 35, 52]. The lower value is typical of low peaks, i.e. late-forming or low-mass objects, while the high value is typical of early-forming or high-mass objects. For comparison, a commonly adopted fiducial Einasto parameter is 0.17 [e.g. 55]. The NFW profile should be intermediate, and most similar to an Einasto profile with $\alpha \sim 0.2$ –0.25. We will use units $G = 1$, $r_{\text{unit}} = r_{-2}$, and $M_{\text{unit}} = M_{\text{NFW}}(r < 10 r_{-2})$; i.e., of profiles will be normalized to have the same virial mass and a concentration of $c = 10$. As shown in Figure 2, though these profiles have the same virial mass and concentration, at radii less than 10 per cent of scale radius, the central densities begin to differ considerably.

We will primarily use the Energy Truncation method to describe our tidally stripped systems and compare these results to two commonly used approximations in the literature: (1) the H03 model and (2) a sharp truncation (ST) of an NFW model. The H03 model is known to underestimate the central density, while the ST model preserves the NFW profile precisely within the tidal radius. These two approximations of a tidally-stripped NFW profile will therefore serve as limiting cases. The parameterizations by [69] and [36] are expected to

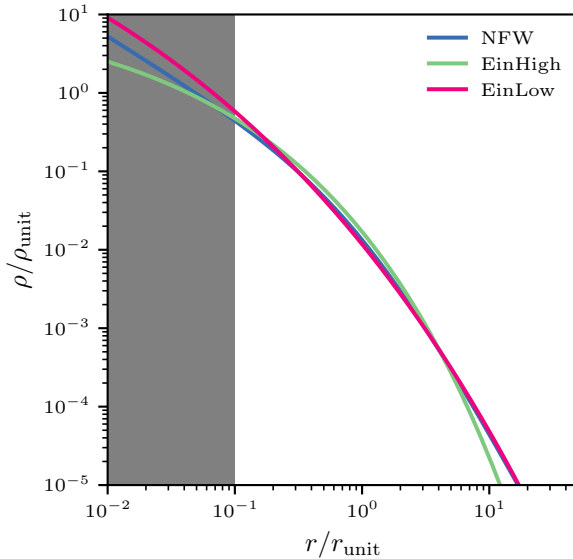


Figure 2. Comparison of initial, unstripped profiles used in this work. All of these are normalized to have the same virial mass and a concentration of $c = 10$. At radii smaller than approximately 10 per cent of the scale radius (grey box)—which are beyond what is typically resolved in isolated simulations—there is a significant difference in the central density of the different models.

Table 1. Summary of the subhalo models used in this work. For all models, subhaloes are assumed to have an infall mass of $M_{\text{unit}} = M_{\text{NFW}}(r < 10 r_{-2})$ and a concentration of $c = 10$.

Profile Name	Initial Profile	Stripping Model
NFWT	NFW	Energy Truncation
EinHighT	EinHigh	Energy Truncation
EinLowT	EinLow	Energy Truncation
ST	NFW	Sharp truncation
H03	NFW	Parametric model from [39]

fall somewhere between the Energy Truncation model and the H03 model.

A summary of the models for describing the tidally stripped systems is given in Table 1, and Figure 3. These models will allow us to compare

1. Differences in predictions caused by assumptions about the initial profile model; i.e., between NFWT, EinHighT, and EinLowT
2. Differences in predictions caused by assumptions of how a tidally stripped profile evolves, i.e., between NFWT, H03, and ST.

3 Evolution of the concentration parameter

Density profiles can be characterized by a concentration parameter, which reflects the distribution of mass within the system. For isolated haloes, the concentration parameter c is

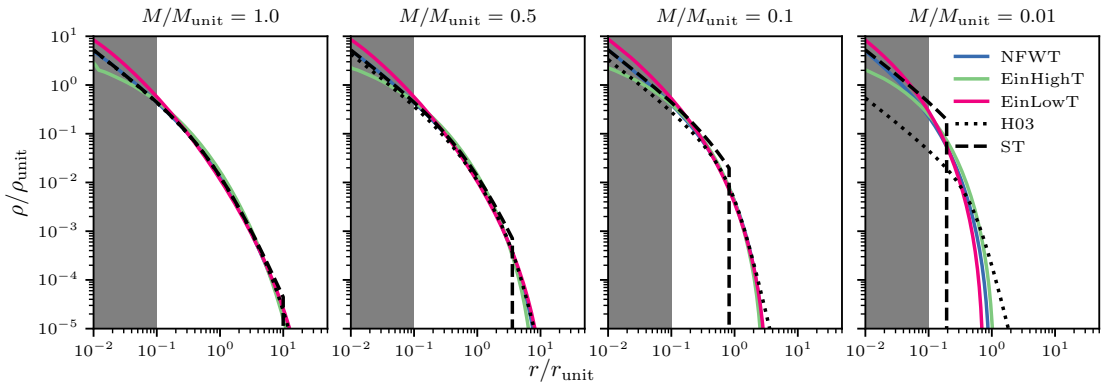


Figure 3. Tidally stripped subhalo density profiles. The models are summarized in Table 1. Each panel is tripped to a different bound mass. As in Figure 2, the grey box indicates radii that are beyond what is typically resolved in isolated simulations. The Energy Truncation model predictions (NFWT, EinHighT, and EinLowT) are similar, except at very small radii. The two other stripping models differ significantly from the Energy Truncation model. The H03 model underestimates the density of the subhaloes at small mass fractions, while the ST model only agrees with NFWT at small radii.

traditionally defined in terms of the radius at which the logarithmic density profile has a slope of -2 , i.e., $c = r_{\text{vir}}/r_{-2}$ [63], where r_{vir} is the virial radius. As discussed in [29, 52], this definition can be problematic for general cases, as it does not capture deviations from an NFW profile. Several other definitions of concentration exist, but the relationship between them is profile-dependent. Thus we will restrict ourselves to the traditional definition, taking the ratio of r_{vir} and r_{-2} .

In cosmological simulations, the virial radius is normally defined in terms of a (redshift-dependent) mean enclosed density. In idealized merger studies, the definition of the virial radius is somewhat arbitrary, but as in Section 2.3, we assume the satellite haloes begin merging with a concentration of $c = 10$. This corresponds to an over-density of $\bar{\rho}_{\text{vir}} = 0.2387 \rho_{\text{unit}}$. As the satellite is stripped, we solve for r_{vir} as the radius where the $\bar{\rho}(r_{\text{vir}}) = \bar{\rho}_{\text{vir}}$. The scale radius, r_{-2} , is calculated directly by numerically differentiating and then solving $d \log_{10} \rho / d \log_{10} r = -2$.

As we will show below, this first definition of concentration generally *increases* as mass is lost since the scale radius shrinks faster than r_{vir} . While this definition is useful for tracking how the bound remnant of a subhalo increases in mean density as it loses its lower-density outer material, r_{vir} has no clear physical significance once a halo has become a subhalo since its density no longer tracks the original cosmological mean value. Thus, in addition to the classical concentration, $c = r_{\text{vir}}/r_{-2}$, for stripped systems we will consider an “effective” concentration parameter, $c_t = r_t/r_{-2}$. As argued in [4, 68], this definition may be more natural as it better reflects the higher mean density of subhaloes and the lower concentration the subhalo had when it was originally accreted. In general, we define the tidal radius r_t to be the radius at which the density profile is zero. With this definition, the H03 profile does not have a tidal radius, so for this profile, we will instead use the effective tidal radius, r_{te} , as defined in Equation (2.3).

With these definitions, Figure 4 shows the evolution of the scale radius, the virial radius, the tidal radius, and the two concentration parameters as the bound mass fraction decreases

from left to right on the x axis. For all three Energy Truncation models (NFWT, EinHighT and EinLowT) the scale radius decreases monotonically as the halo is tidally stripped, as expected [27]. The relative change in r_{-2} is always slower than the relative mass loss rate, however, such that when the system has lost 90% of its mass, r_{-2} has only decreased to 20–50 per cent of its initial value. The behaviour for the evolution of r_{-2} the H03 approximation is similar, although this model generally predicts a scale radius that is 10–50 per cent higher than the Energy Truncation model. The ST approximation predicts a constant r_{-2} until the tidal radius is less than the scale radius (at approximately $0.5 M_{\text{unit}}$), at which point the evolution of the scale radius is similar to the Energy Truncation models.

The virial radius shows a similar monotonic decrease that is approximately the same for all three Energy Truncation models; it varies only because of the slightly different relationship between mean density versus radius for each profile. Once again, r_{vir} changes more slowly relative to its initial value than the bound mass.

The tidal radius, r_t , also decreases with mass, however—unlike r_{vir} —the value of r_t varies widely between the models. For the three Energy Truncation models, r_t is initially very large and decreases rapidly until the mass is approximately 10 per cent of M_{unit} . At smaller masses, the three Energy Truncation models agree quite well. The H03 and ST approximations do not agree with Energy Truncation models and, instead, look similar to each other. Both of these approximations start with $r_t = r_{\text{vir}}$ and then rapidly decrease. We emphasize that the tidal radius is defined differently for the H03 model, using the parameter r_{te} . This effective tidal radius is used in the H03 parameterization but does not have a clear physical meaning. We also note that the “virial” radius is typically larger than the tidal radius, except for the Energy Truncation models at high mass fractions; this means the virial radius is simply given by $r_{\text{vir}} = (4\pi\bar{\rho}_{\text{vir}}/3M)^{1/3}$.

Taking the ratio of the two outer radii to the scale radii, we calculate corresponding concentration parameters. For the Energy Truncation models, $c = r_{r_{\text{vir}}}/r_{-2}$, increases with decreased mass. We emphasize however that this apparent increase in c comes from the definition of the virial radius, which tracks the original density of the system and ends up outside the actual tidal radius. Physically, the material still bound to the subhalo within its tidal radius is less concentrated — this is better captured by the second concentration parameter, c_t . We show how the second effective concentration parameter varies with mass loss in the bottom panel of Figure 4. Once the subhaloes have been stripped to about 20% of their original mass, the effective concentration is approximately constant at $c_t \approx 10$. Given the faster decline in its scale radius, the EinLowT profile has higher concentrations than the NFWT and EinHighT profiles. The ST and H03 models under-predict c_t by an order of magnitude or more, though in the case of the H03, this is largely because the tidal radius definition is different.

Overall, all profiles and mass loss models show certain broad trends. Stripped subhaloes have higher densities than field haloes of the same mass, but their bound material is more uniformly distributed than that of field haloes. Thus, concentrations relative to the original virial boundary generally increase, while concentrations relative to the tidal radius decrease. Nonetheless, there significant differences in concentration evolution are predicted simply based on differences in (1) the initial profile model and (2) the tidal stripping model. Finally, we note that the Energy Truncation model predicts that at low bound mass fractions, the scale radius and tidal radius will evolve at similar rates, resulting in a constant c_t value.

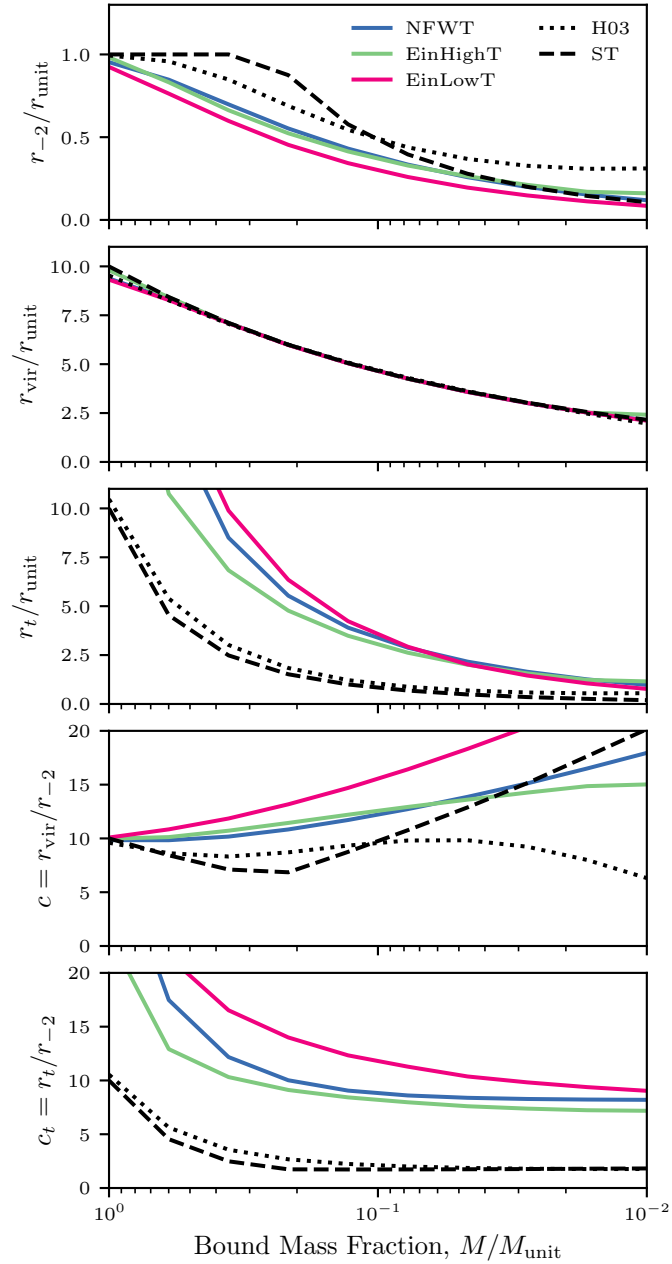


Figure 4. Evolution of the parameters used to characterize subhalo concentration as a function of mass fraction, for various profiles: (1) the scale radius r_{-2} , (2) the virial radius r_{vir} ; the radius enclosing an overdensity of $\bar{\rho}_{\text{vir}} = 0.2387 \rho_{\text{unit}}$ (3) the tidal radius (4) the concentration parameter $c = r_{\text{vir}}/r_{-2}$, and (5) the effective concentration $c_t = r_t/r_{-2}$. All three Energy Truncation models evolve similarly to each other, with the EinLowT concentration being about 20 per cent higher than the NFWT, and EinHighT models. The concentration parameters calculated from two approximate models, H03 and ST, evolve quite differently.

4 Dark matter annihilation

One potential technique for determining the identity of dark matter particles is through dark matter annihilation. To place constraints on particle masses and interaction cross-sections, it is important to have accurate predictions of the distribution of dark matter within subhaloes, since the dark matter annihilation signals depend sensitively on substructure. Assuming the dark matter particles are Majorana WIMPs (weakly interacting massive particles) that can annihilate with one another, the rate at which dark matter annihilates is given by:

$$R = \frac{\langle\sigma v\rangle}{2m^2} \int_V \rho^2 dV , \quad (4.1)$$

where $\langle\sigma v\rangle$ is the velocity-averaged annihilation cross section, m is the mass of the dark matter particle, ρ is the density and V is a volume [e.g. 80]. Thus, the annihilation rate is proportional to the quantity

$$J \equiv \int \rho^2 dV , \quad (4.2)$$

which is sometimes called the J -factor², and has dimensions mass \times density. This quantity is sensitive to the high-density inner region of the halo and does not vary with the choice of integration volume as long as the volume is large enough to enclose the region of high density.

Since the J -factor depends on the overall size and mass of the system, it is also convenient to define a dimensionless quantity,

$$B(V) = \frac{1}{\bar{\rho}^2 V} \int \rho^2 dV , \quad (4.3)$$

which is often called the boost factor.³ Unlike the annihilation rate, the boost factor is sensitive to the integration volume. In the case of CDM haloes, it is common to use the spherical volume within the virial radius. The boost factor is useful in calculating the total annihilation signal from a system; a common approach is to draw subhalo properties such as infall redshift, mass, concentration, and/or orbital properties from random distributions, and then use the boost factor to calculate the contribution from each subhalo to the total signal [e.g. 4, 17, 34, 37, 40, 43, 44, 68, 76, 77].

In terms of the boost factor, the annihilation rate can be expressed as:

$$R(V) = \frac{\langle\sigma v\rangle}{2m^2} \bar{\rho}^2 V B(V) , \quad (4.4)$$

where the first term, $\langle\sigma v\rangle/2m^2$, depends on the particle physics of the dark matter candidate, the second term $\bar{\rho}^2 V$ depends on the mean density and volume (or equivalently the mean density and total mass) of the system, and $B(V)$ characterizes the inhomogeneity of the particle distribution within the volume V .

The boost factor (top) and J -factor (bottom) calculated within a spherical volume of radius r are shown in Fig 5 for each profile model and various degrees of mass loss. For the boost factor (which is a measurement of how inhomogeneous the mass distribution is), the parameter is roughly constant within the scale radius, r_{-2} , and then increases rapidly

²Here we follow the definition of [14]; more commonly the J -factor is expressed as a projected quantity.

³Not to be confused with the substructure boost factor, which is the luminosity of the signal divided by the luminosity from the smooth host halo [68].

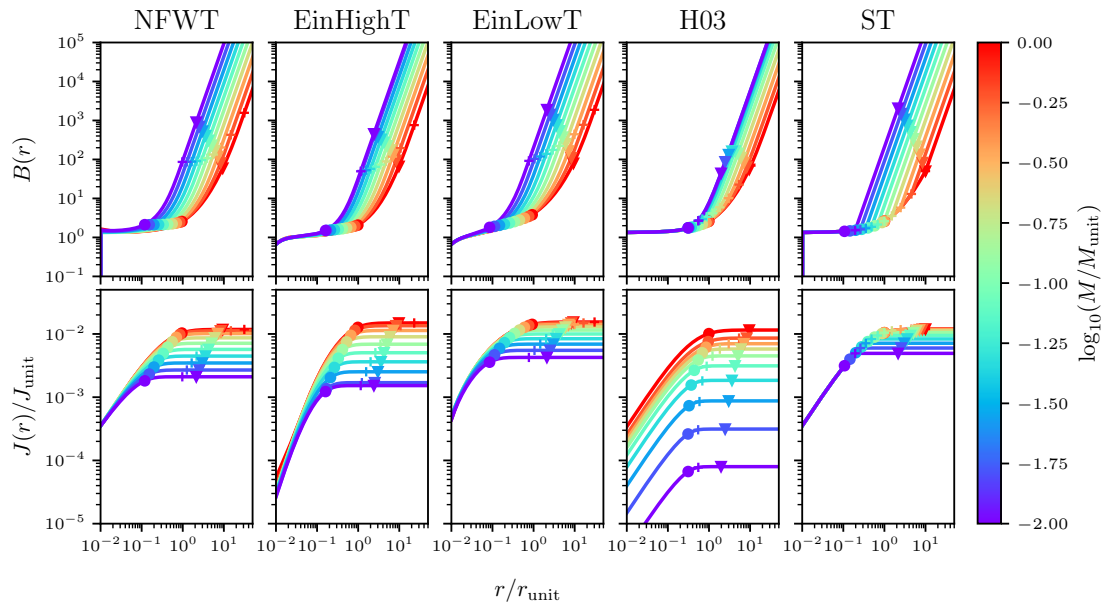


Figure 5. The boost factor (top) and J -factor (bottom) for tidally stripped subhalo models, as a function of the radius of the spherical volume within which the integral is calculated. The colour scale indicates the degree of stripping. The characteristic radii r_{-2} , r_{vir} and r_t are labelled as circles, triangles, and crosses, respectively. The boost factor is approximately constant within the scale radius and then increases as r^3 . Conversely, the J -factors increase rapidly within the scale radius and then are constant at large radii. This plot demonstrates how the boost factor and J -factor measurements depend on the choice of integration volume.

with radius (with $B \propto V$ outside the tidal radius). Inside r_{-2} , there is little evolution in the boost factor as mass is stripped, while outside this radius, the boost factor is higher for more stripped systems. Conversely, the J -factor increases with a radius for $r < r_{-2}$ and then is approximately constant at larger radii, but its value decreases as the system is stripped, especially in model H03.

4.1 Boost Factor Evolution

In the top row of Figure 6, we show how the boost factor evolves as a function of bound mass using different volumes. As expected from Figure 5, when calculated within the scale radius, the boost factor stays roughly constant. Within the virial radius—except the H03 approximation—the boost factor increases as mass is stripped. Finally, within the tidal radius, the boost factor *decreases* as the profile is stripped, with both the H03 and ST approximation having a lower boost factor by two orders of magnitude. This difference is largely because of the different volumes in which the boost factor is calculated. If we focus on the evolution of the boost factor relative to its initial value (second row), this difference disappears.

It is also worth comparing predictions of boost factors to the values obtained using the untruncated profile. The bottom row of Figure 6 shows the ratio B/B_{un} , where B_{un} is the initial un-truncated profile. We compare our findings to the constant value of 1.3, since [80] showed that the H03 model follows the relation $B \simeq 1.3 B_{\text{un}}$ when measured within r_{te} .

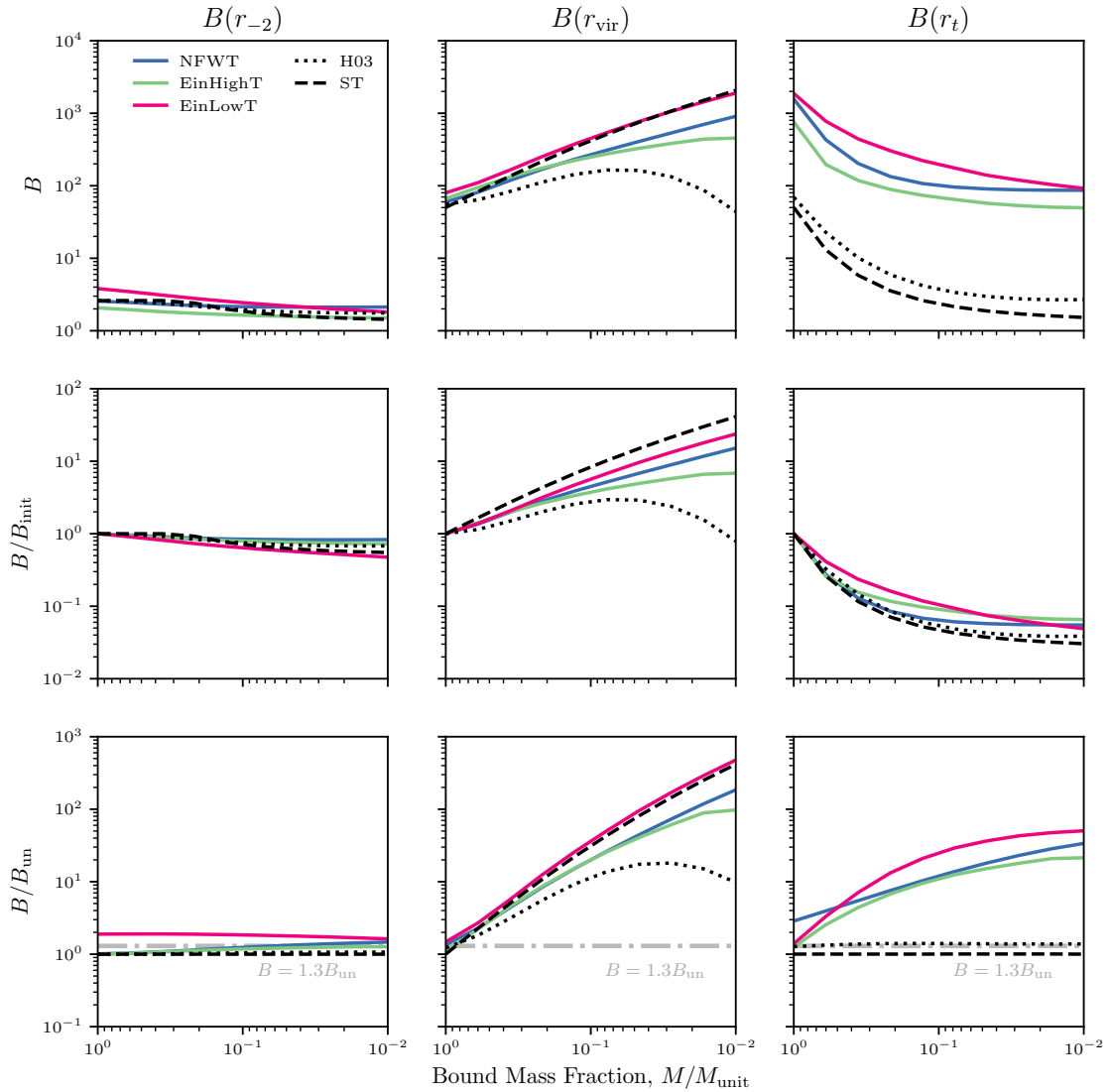


Figure 6. Evolution of the boost factor calculated within different volumes. The top row shows the boost factor, the second panel shows the evolution from the initial value, and the bottom shows the ratio between the boost factor of the tidally-stripped profiles and the initial, untruncated profiles.

When measured inside the scale radius, the boost factor is constant for all models and consistent with $B = 1.3B_{\text{un}}$. When measured within the virial radius, we find much higher values of B/B_{un} . This result is because the virial radius is typically larger than the tidal radius in these systems. Since mass loss reduces the density in the outer parts of the stripped halo, this makes the density distribution of stripped systems more centrally concentrated and less homogenous, and thus it increases B .

When measured within the tidal radius, we find the ST and H03 approximations agree with the $B \simeq 1.3B_{\text{un}}$ prediction, as expected. The more accurate Energy Truncation stripping models predict a boost factor that is more than 10 times higher by the time the bound mass fraction is less than 10 per cent. We conclude that the boost factor is extremely sensitive to

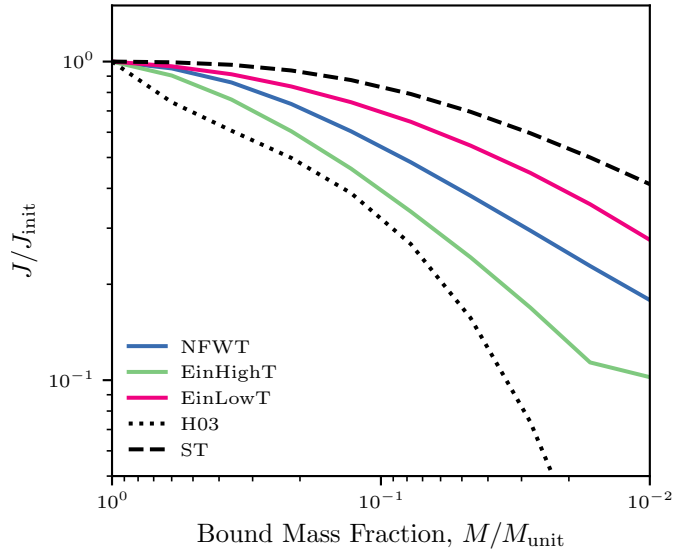


Figure 7. Change in the J -factor versus bound mass fraction predicted from our models. There are large differences between all of the models, suggesting that J -factor predictions are very sensitive to assumptions about subhalo profiles. Further, the J -factor is not constant as is often assumed but can decrease significantly by the time the subhalo is stripped to half of its mass.

the details of mass loss within the tidal radius, and may have been underestimated in previous work. Thus, it may not provide the best way to calculate the annihilation signal

4.2 J -Factor Evolution

Ultimately we are interested in predicting the total annihilation rate in dark matter subhaloes, which is proportional to the J -factor defined in Equation 4.2. In Figure 7, we show predictions for how the J -factor evolves with mass loss for the different profile models. We calculate the J -factor within the tidal radius but note that the J -factor is insensitive to this choice. As with the boost factor, we find large differences in the J -factor between the different models. By the time the profile is stripped to 5 per cent of the initial mass, there is a factor of 5 difference in the annihilation signal between the ST approximation and the H03 approximation, while the Energy Truncation predictions lie between the two. It is often assumed that since the high-density inner regions of subhaloes are resilient against tidal forces, the annihilation rate will remain fairly constant during tidal stripping [4]. Figure 7 shows that this assumption is incorrect, once mass loss reaches a significant level.

Comparing the three Energy Truncation models, the EinLowT J -factor (whose density profile has a steeper central cusp; Figure 2) decreases the least, while the value from the flatter EinHigh profiles decreases the most. The ST model (dashed line) always overestimates the annihilation signal. Although the H03 model (dotted line) gives a reasonable match to the stripped density profile except at very low masses/radii (Figure 3), this model predicts much lower annihilation rates overall.

The variation in the predicted J -factor between models reflects the sensitivity of the

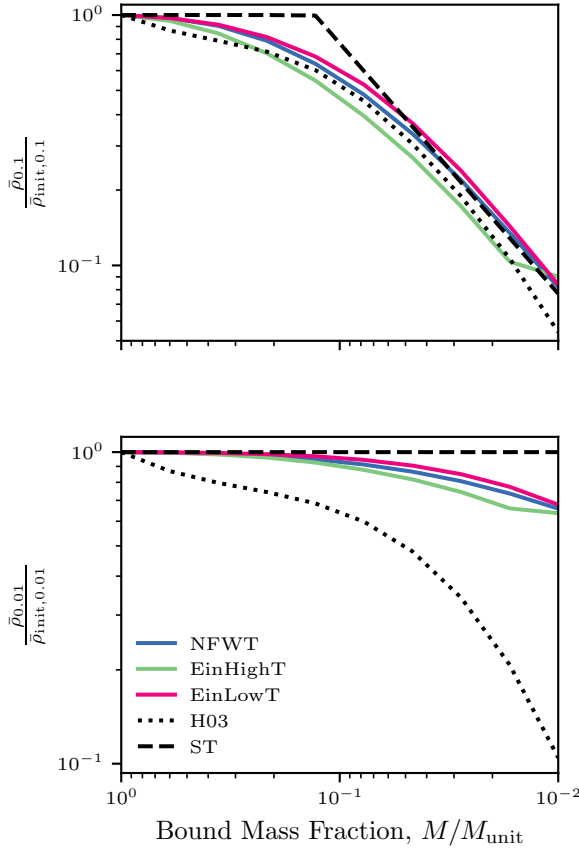


Figure 8. Change in the central density versus bound mass fraction for various profiles. The enclosed density is calculated in either 10 per cent (top) or 1 per cent (bottom) of the initial virial radius. The enclosed density decreases over time, with slight differences between the three Energy Truncation profiles. For the ST approximation, the enclosed density is constant over time within the tidal radius and thus over-predicts the more accurate NFWT model. The H03 approximation predicts a large decrease in the central density and thus under-predicts the NFWT model.

annihilation signal to the central density. In Figure 8 we show how the enclosed central density evolves with bound mass. We consider the mean density within 10 per cent ($\bar{\rho}_{0.1}$; top panel) and 1 per cent ($\bar{\rho}_{0.01}$; bottom panel) of the initial virial radius (as described in Section 3). The cuspy EinLow profile has the smallest change in central density, which is why the J -factor for this model changes slowly. When comparing approximations for tidally stripped NFW profiles, the central density of the ST model is constant as expected, as long as the tidal radius exceeds the radius used to calculate the enclosed density. Relative to the NFW results, both the ST and the H03 model do a fairly good job at predicting the enclosed density within 10 per cent of the virial radius. However, the ST approximation over-predicts the central density within 1 per cent of the virial radius, while the H03 approximation greatly under-predicts the enclosed density, as discussed in Section 2.3.

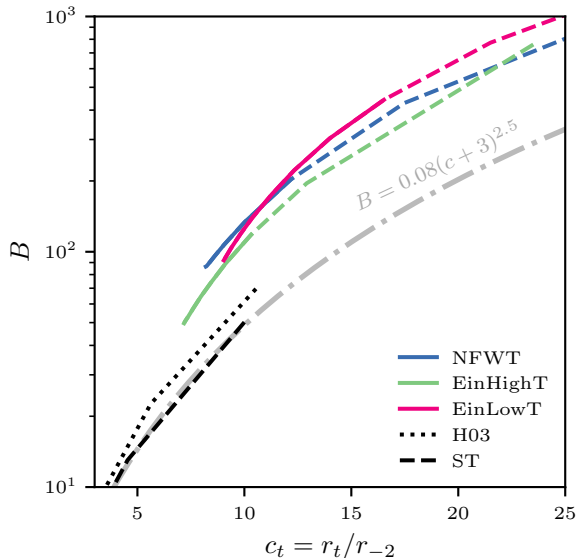


Figure 9. Boost factor as a function of the effective concentration parameter, $c_t = r_t/r_{-2}$. For comparison, we show the expected relation for an unstripped NFW profile (dotted gray line), using the parameterization from (author?) [68]. Note that for the Energy-Truncation models, there are some cases where $r_t > r_{\text{vir}}$, and therefore not a physically accurate depiction of the concentration. We denote cases where $r_t > 10r_s$ with a dashed line. Overall, we find that the Energy Truncation models have boost factors at least twice as large as expected from the unstripped profiles; this is contrary to the expectation that the boost factor of the stripped profile should be approximately equal to that of the unstripped profile within the tidal radius.

4.3 Dependence on structural parameters

For an NFW profile, the boost factor can be well-approximated as a function of the concentration parameter $c = r_{\text{vir}}/r_{-2}$ alone, with $B \sim c^{2.5}$, while the boost factor for Einasto profiles scales similarly with a slight dependence on the shape parameter α [68]. For tidally stripped haloes, r_t is a more natural outer radius, as discussed in Section 7. In Figure 9, we show the relationship between the boost factor and the effective concentration parameter, c_t . We also compare this relation to the [68] parameterization for how B varies with c for an untruncated NFW profile (the dash-dot grey line). As mentioned in [68], we expect that $B(c_t)$ should be approximately equal between the unstripped and stripped profiles since most of the mass is removed outside the tidal radius. We find that though $B(c_t)$ matches the un-truncated NFW calculation for the H03 and ST models, our three Energy Truncation models have much higher boost factors for a given tidal radius, as shown previously in Figure 6.

The J -factor and structural properties of subhaloes are also known to be related. For instance, [14] examined the relationship between J and $G^{-1}v_{\text{max}}^4 r_{\text{max}}^{-1}$, where v_{max} and r_{max} are the maximum circular velocity ($v_c = \sqrt{GM(< r)/r}$), and corresponding radius. They show that while for an NFW profile $\log_{10} J = 1.23 \log_{10}(G^{-1}v_{\text{max}}^4 r_{\text{max}}^{-1})$, their tidally-stripped simulations of NFW profiles have a slightly shallower slope of 0.86. Our NFWT model agrees remarkably well with their findings, but differences in the profile model can cause a difference in the J -factor by an order of ≈ 2 .

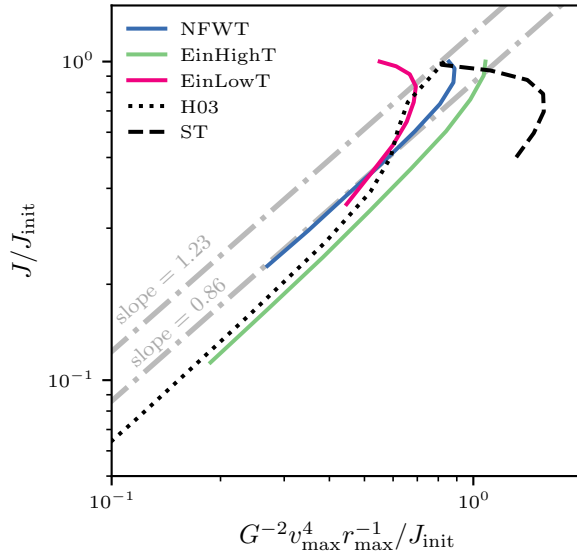


Figure 10. Relationship between the J -factor, and the combination of structural parameters $G^{-1}v_{\max}^4 r_{\max}^{-1}$, where v_{\max} and r_{\max} are the maximum circular velocity. The slope of 1.23 is what is expected for an NFW profile, while 1.86 is what has been found for tidally stripped NFW profiles [14]. We find that our NFWT model agrees with this scaling relation, but differences in initial profiles can cause a deviation in the J -factor by factors of ≈ 2 .

4.4 Model Sensitivity in Annihilation: Summary

In this section, we considered the effects of tidal mass loss on the inner structure of subhaloes as they relate to calculations of the annihilation rate. Assuming a truncation of the distribution function in energy space, we calculated quantities related to the dark matter annihilation rate for NFW, EinHigh, and EinLow profiles. Additionally, we compared our prediction for NFW profiles to two widely used approximations; first, a model in which the original NFW profile is sharply truncated such that it contains the same bound mass (ST model), and secondly, the parameterization from [39] that was tuned to simulation results (H03).

Comparing first the energy-truncated NFW and Einasto profiles, we found that for fixed mass, the concentration, boost factor (measured within the tidal radius), and J -factor of the EinLowT profile is typically 10-50 per cent higher than the NFWT profile, while the EinHighT profile is typically lower. These differences reflect the different central densities of the initial models, as the annihilation signal is dominated by these high-density regions.

Then, comparing tidal stripping models (the NFWT model versus the commonly used ST and H03 approximations), we found that neither of the common approximations agrees well with the Energy Truncation model. The effective concentration is lower by a factor of 10 for both approximations. Both models under-predict the boost factor within the tidal radius by a factor of ~ 100 . However, this result is mainly due to the differences in the tidal radii, and if we consider the evolution of B/B_{init} the H03 and ST model underestimate and overestimate the boost factor by ~ 20 per cent, respectively. If we consider the B/B_{un} ; i.e.,

the boost factor from our model compared to a truncated profile within the same radius, r_t , we can find that the two approximations underestimate the boost factor by an order of magnitude. Overall, the J -factor is overestimated in the ST model and underestimated in the H03 model; the differences between these models are a factor of 5 once the halo has been stripped to $\sim 5\%$ of its initial mass.

In summary, subhalo concentrations, boost factors, and J -factors of tidally stripped haloes are sensitive to the innermost part of the density profile, and predicted fluxes can vary by a factor of 5 or more depending on profile assumptions. Thus, it is important to have physically motivated models, such as the Energy Truncation model, that allow us to predict the annihilation of subhaloes down to arbitrarily small bound mass fractions. Our results suggest that current constraints on the CDM annihilation cross-section may be inaccurate due to their underlying assumptions about subhalo density profiles; addressing these inaccuracies will be the focus of future work.

4.5 Implications for the Milky Way

We provide a brief exploration of what our results mean in the context of the Milky Way galaxy — more robust calculations will be the focus of future work. Throughout this section, we assume the Milky Way has a virial mass of $M_{\text{MW}} = 10^{12} M_{\odot}$, a virial radius of 250 kpc, and a concentration of 10. We use a Planck 2018 cosmology [71].

The total Milky Way annihilation signal can be expressed as

$$J_{\text{MW}} = J_{\text{sub}} + J_{\text{strip}} , \quad (4.5)$$

where J_{sub} is the annihilation signal due to Milky Way subhaloes at redshift $z = 0$ and J_{strip} is the annihilation signal from the stripped mass.

The signal from the substructure can be found by adding the contribution from each subhalo,

$$J_{\text{sub}} = \int_{\infty}^0 \int_{M_{\text{min}}}^{M_{\text{max}}} \frac{dN}{dM_i dz} J(M_0) dM_i dz , \quad (4.6)$$

where N is the number of haloes, M_i is the mass of a subhalo at infall redshift, z , and M_0 is the mass of the subhalo at redshift 0. The annihilation signal of each subhalo, $J = J(M_0)$, depends on the assumed density profile of the subhalo. We assume a minimum halo mass of $10^{-6} M_{\odot}$, as in [68].

To calculate J_{strip} , we assume that the stripped mass is smoothly distributed in an NFW profile, and is given by:

$$M_{\text{strip}} = \int_{\infty}^0 \int_{M_{\text{min}}}^{M_{\text{max}}} \frac{dN}{dM_i dz} (M_i - M_0) dM_i dz . \quad (4.7)$$

To find the relationship between the infall mass and the current mass of the subhaloes, we use [48]:

$$M_0 = M_i \exp\left(\frac{-0.81\sqrt{200}z_i}{\pi}\right) , \quad (4.8)$$

where z_i is the infall redshift, and we calculate J_{sub} using different models for the subhalo density profiles. However, we note that this parameterization is likely an overestimate of the mass loss, and does not take into account the effect of subhalo structure on mass-loss rates.

Finally, we assign concentrations to subhaloes assuming they lie on the median concentration–mass relation from [46].

We calculate $dN/dM_i dz$ by assuming the infall population is the same as the field population:

$$\frac{dN}{dM_i dz} = \frac{1}{\rho_c(z)} \frac{dM_{\text{MW}}(z)}{dz} \frac{dn}{dM} , \quad (4.9)$$

where $dn(M, z)/dM$ is the [20] halo mass function, $M_{\text{MW}}(z)$ is the mass of the Milky Way at redshift z , and ρ_c is the critical density. We assume the Milky Way mass evolves according to [87]:

$$M_{\text{MW}}(z) = M_{\text{MW}}(0) \exp(-8.2z/c) . \quad (4.10)$$

The top panel of Figure 11 shows the relative contribution of substructure to the total annihilation signal, as a function of subhalo mass. The signal is dominated by the smallest subhaloes, with approximately 70 per cent of the signal coming from haloes less than $10^6 M_\odot$. The contribution of subhaloes to the total annihilation signal differs slightly between models, with small subhaloes in more centrally concentrated models contributing slightly more to the annihilation signal.

Then, we compared the ‘substructure boost factor’ [68] — defined as the annihilation flux from substructure, J_{sub} relative to the flux from the smooth component of the halo — in the bottom panel Fig 11. We calculated the smooth component by assuming all of the Milky Way mass was smoothly distributed in an NFW profile with mass

$$M_{\text{tot}} = \int_{-\infty}^0 \int_{M_{\text{min}}}^{M_{\text{max}}} \frac{dN}{dM_i dz} M_i dM_i dz . \quad (4.11)$$

We find that including substructure increases the signal by a factor of ~ 50 for the more centrally concentrated profiles (ST and EinLowT), and ~ 10 times for the less centrally concentrated profiles (H03). The lower values are comparable to the predictions of [68], who explored different concentration–mass relations, but found a substructure boost factor of ~ 16 when assuming a H03 model and concentration relations similar to ours⁴. This demonstrates the overall importance of substructure in calculating the annihilation signal in the Milky Way, but also the large range of values predicted depending on the assumed subhalo density profile. Assuming low-mass subhaloes have profiles closest to the EinLowT or NFWT models, we predict a ‘substructure boost factor’ of as much as 20–50, relative to the contribution from the smooth halo.

We note, however, that there are several simplifications in this analysis. First, our parameterization for subhalo stripping (Equation 4.8) overestimates how quickly profiles are disrupted. Second, we assumed that all haloes lie on the median concentration–mass relation and that the Milky Way has built up its mass at an average rate. Finally, the rate at which haloes are stripped is dependent on the subhalo model, with cuspiest profiles experiencing less stripping — this, however, would *increase* the difference between the models. We leave a full investigation of how subhalo evolution affects the annihilation signal for future work.

⁴We note that our quantity is slightly different — we are showing the substructure annihilation rate to the smooth signal using the *total* Milky Way Mass, while [68] uses the smooth signal from the mass not contained in subhaloes.

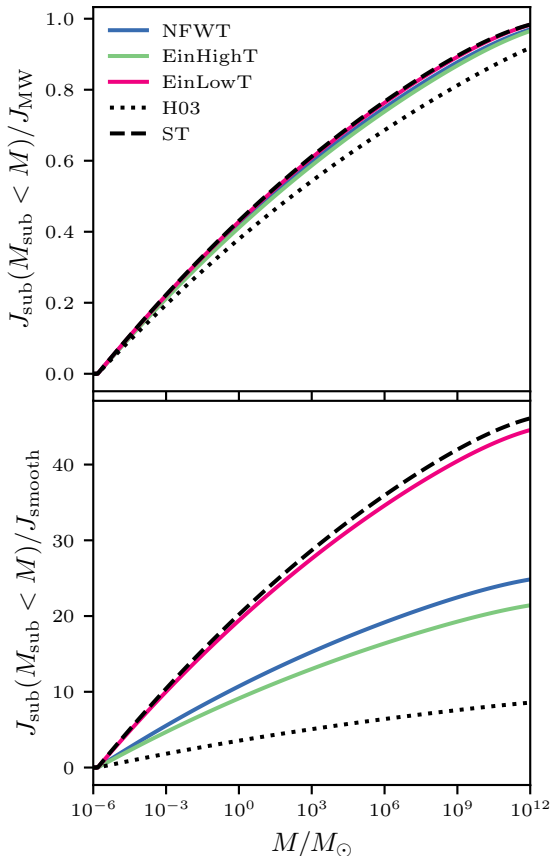


Figure 11. *Top:* Cumulative fraction of the Milky Way annihilation signal contributed by substructure, as a function of subhalo mass. The majority of the signal comes from sub-galactic subhaloes, while there is little difference in the mass dependence between the different subhalo models. *Bottom:* ‘Substructure boost factor’, the annihilation rate from the Milky Way including substructure, relative to the rate if all the mass were distributed smoothly as an NFW profile. Including substructure can increase the annihilation rate by a factor of 10–50, depending on the subhalo model used.

5 Lensing

In gravitational lensing, an image of a background galaxy will be distorted by mass along the line of sight. The mapping between the source and image plane for a background galaxy (i) and its lens (j) is given by the amplification matrix, a_{ij} :

$$a_{ij} = \begin{pmatrix} 1 - \kappa - \gamma_1 & -\gamma_2 \\ -\gamma_2 & 1 - \kappa - \gamma_1 \end{pmatrix}, \quad (5.1)$$

where κ is the convergence and γ is the shear. The corresponding convergence and shear profiles are defined as

$$\begin{aligned} \kappa(R) &= \Sigma(R)/\Sigma_{\text{crit}} \quad \text{and,} \\ \gamma(R) &= (\bar{\Sigma}(\leq R) - \Sigma(R))/\Sigma_{\text{crit}}, \end{aligned} \quad (5.2)$$

for axisymmetric haloes. In the case of multiple lenses, the total amplification matrix can then be calculated by summing the contributions of each lens.

The projected density profile $\Sigma(R)$ can be calculated from the density profile,

$$\Sigma(R) = 2 \int_R^\infty \frac{\rho(r)r}{\sqrt{r^2 - R^2}} dr , \quad (5.3)$$

and the mean projected surface mass

$$\bar{\Sigma}(\leq R) = \frac{M_{\text{proj}}(R)}{\pi R^2} , \quad (5.4)$$

with the projected mass $M_{\text{proj}}(R)$ is given by:

$$M_{\text{proj}}(R) = 2\pi \int_0^R \Sigma(R')R' dR' , \quad (5.5)$$

Finally, the critical surface density, Σ_{crit} is given by:

$$\Sigma_{\text{crit}} = \frac{c^2}{4\pi G} \frac{D_S}{D_L D_{LS}} , \quad (5.6)$$

where D_S , D_L , and D_{LS} are the angular diameter distances from the observer to the source, the observer to the lens, and the lens to the source, respectively. Since Σ_{crit} depends on the geometry of the problem (and consequently the cosmology), it is not well-defined for our isolated simulations. Therefore, in Figure 12 we show Σ and $\Delta\Sigma \equiv \bar{\Sigma} - \Sigma$ for our model, as they are proportional to the convergence and shear, respectively; these profiles can then be scaled appropriately given a value of Σ_{crit} .

In Figure 12, the projected density profiles (top) show similar trends to the 3D density profiles, with $\Sigma(r > r_t) = 0$ (except for H03). The shear profiles (bottom) are approximately constant within the tidal radius and then follow $\Delta\Sigma \propto R^{-2}$. The discontinuity in the slope of the ST model is evident in the shear profiles; the shear is finite but not differentiable at the cutoff radius, as discussed in [3]. Figure 13 shows the evolution of Σ and $\Delta\Sigma$, calculated within $0.5 r_{\text{unit}}$ and $1 r_{\text{unit}}$, as mass is lost. Initially, the EinHighT lens models have slightly higher projected densities than the other models, but generally, all models agree to within 10–20 per cent, except at the discontinuity where the tidal radius is close to the aperture size in the ST model.

5.1 Model Comparisons

To understand better how the convergence and shear depend on the assumed subhalo profile and stripping model, in Figure 14, we compare radial profiles and residuals for the different models. Between $0.1 r_{-2}$ and r_t , EinHighT and EinLowT Σ differ from the NFWT profile by up to 20 per cent, while the shear profiles differ from NFWT profiles by up to 50 per cent. The difference is largest at very small radii, with the EinLowT profile having higher convergence and shear values, due to the increased density in the centre of the profile. We also compare the energy-truncated NFW profiles to the commonly used H03 and ST approximations. The H03 model underestimates the convergence and shear profiles at small radii, though differences between H03 and NFWT are comparable to differences found between the different initial profiles, assuming energy truncation. The ST model closely matches the NFWT model at small radii but is less extended.

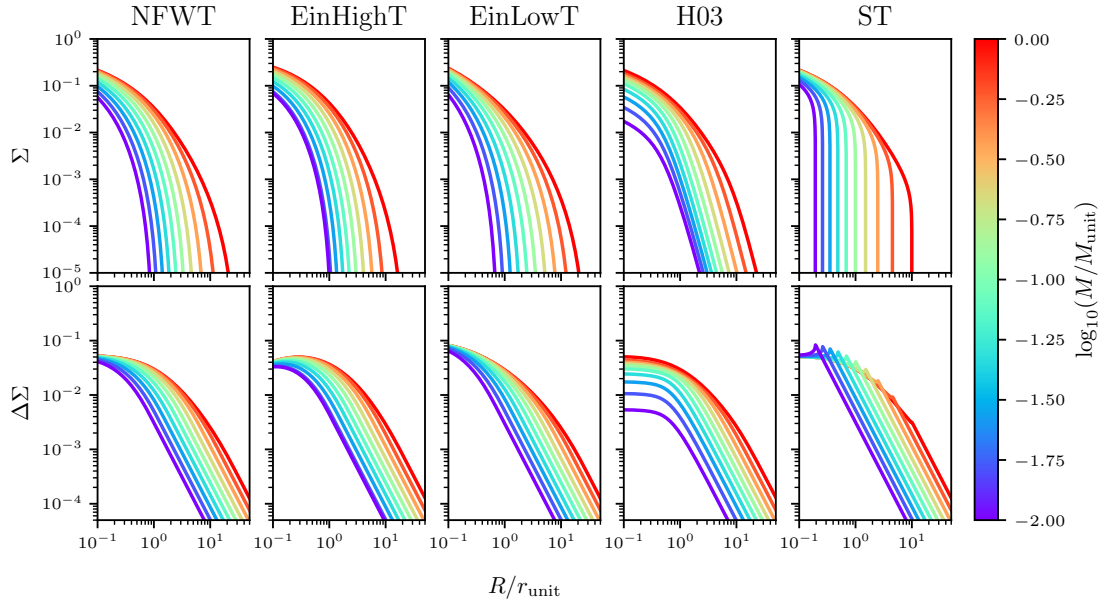


Figure 12. The projected density profile, Σ , (top) and $\Delta\Sigma \equiv \bar{\Sigma} - \Sigma$ (bottom) from our models, as a function of bound mass. Σ is proportional to the convergence, κ , and $\Delta\Sigma$ is proportional to the shear γ for axisymmetric systems.

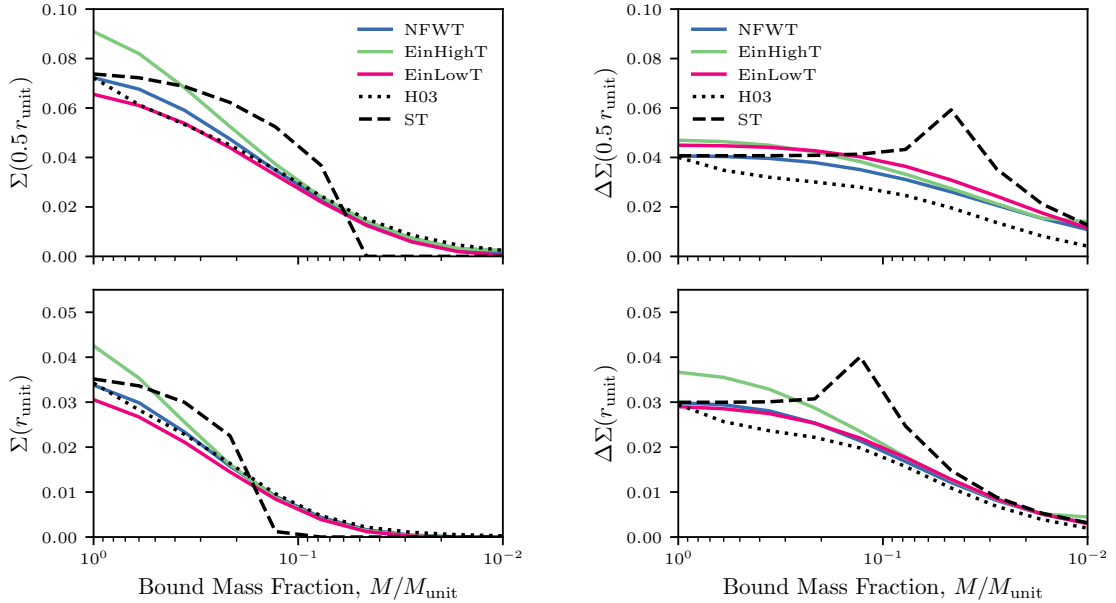


Figure 13. Variation with mass loss in the mean projected density Σ (left) and $\Delta\Sigma$ (right), as measured within apertures of $0.5 r_{\text{unit}}$ (top) or $1 r_{\text{unit}}$ (bottom). Both quantities decrease with mass loss, except for shear in the ST model, which increases when the tidal radius is comparable to the scale radius (initially equal to $1.0 r_{\text{unit}}$). Except at this discontinuity, all models agree to within 10–20 per cent.

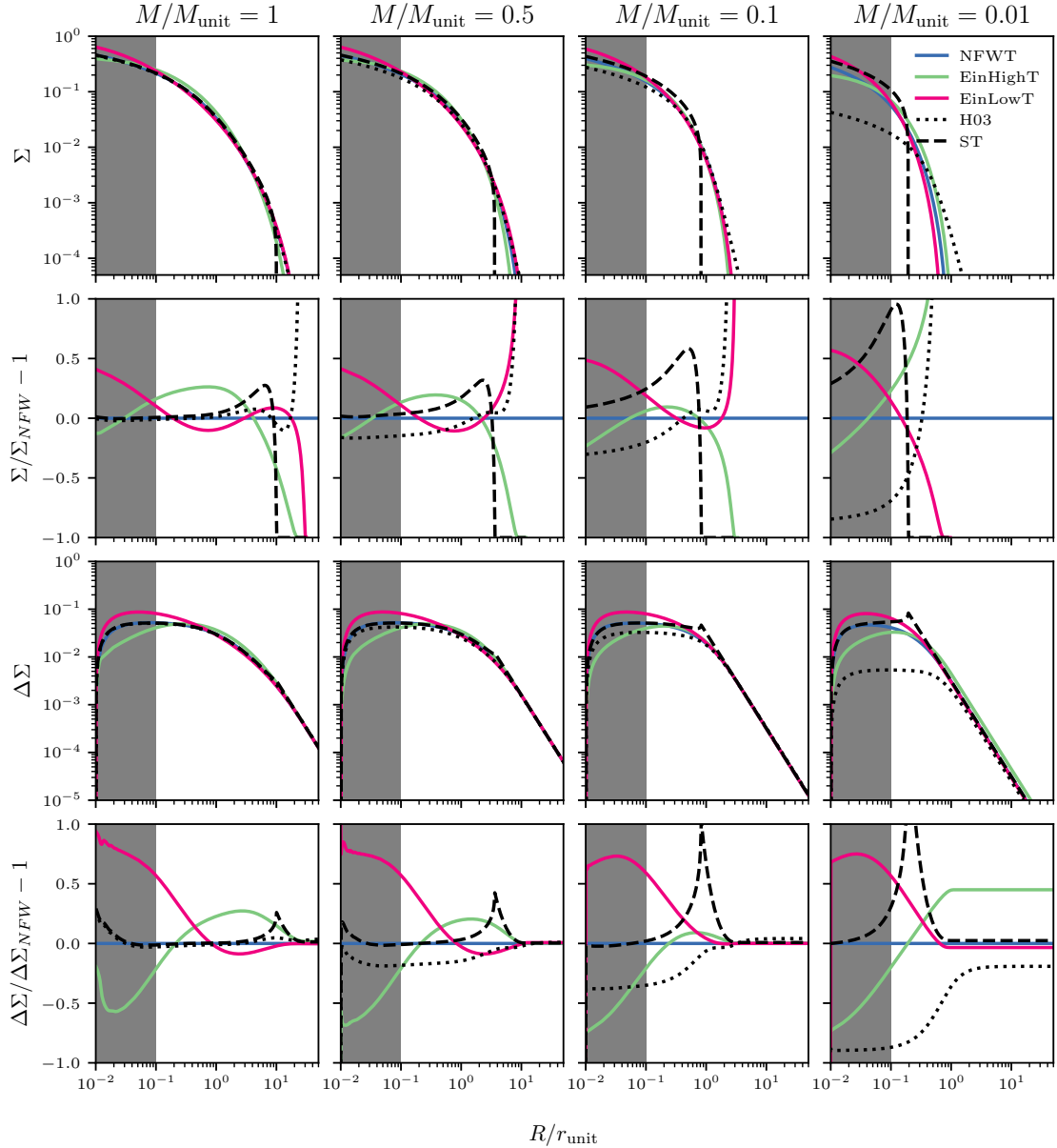


Figure 14. The projected density profile, Σ , (top) and $\Delta\Sigma \equiv \bar{\Sigma} - \Sigma$ (third row) for the Energy Truncation model applied to three different profiles (NFWT, EinLowT and EinLowT), the stripping model from (author?) [39] applied to an NFW profile (H03; dotted line), and a sharply truncated NFW profile (ST; dashed line). Each column corresponds to a different bound mass, as indicated. The second and last rows show the ratio of Σ and $\Delta\Sigma$, respectively, to the NFWT model. The grey box indicates radii that are typically unresolved in isolated simulations. There are significant differences between the three initial halo models, but the ST approximation does a good job of approximating the NFWT profiles, except for $\Delta\Sigma$ measured close to the truncation radius.

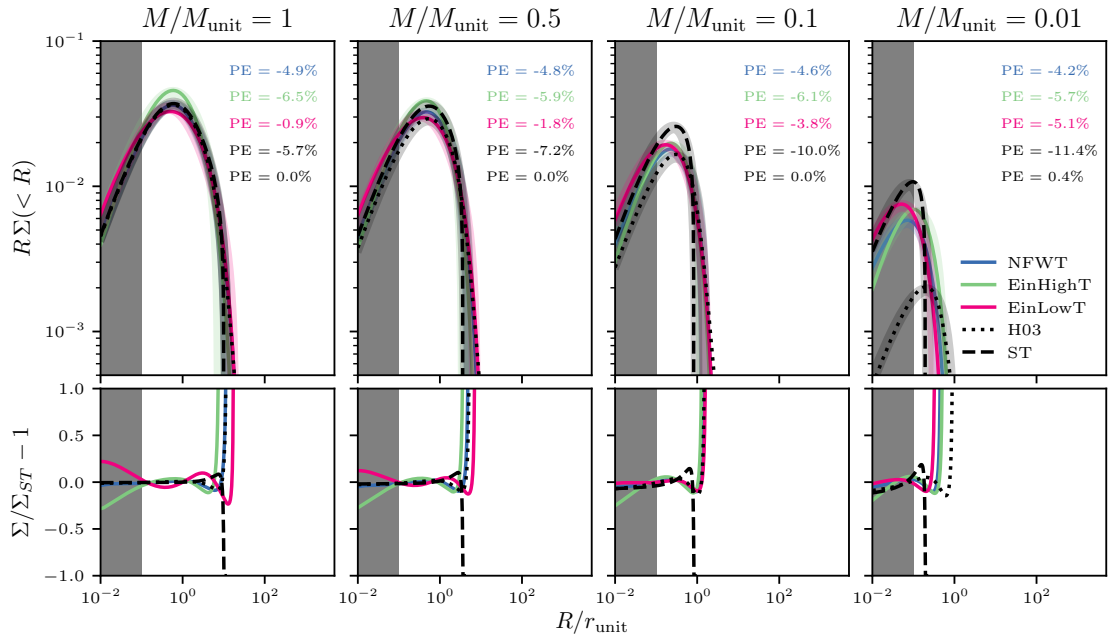


Figure 15. *Top:* The projected density profile, Σ for the Energy Truncation model applied to three different profiles (NFWT, EinLowT, and EinLowT), the stripping model from (author?) [39] applied to an NFW profile (H03; dotted line), and a sharply truncated NFW profile (ST; dashed line). Each column corresponds to a different bound mass, as indicated. The thick transparent lines are the best-fit ST models. We also show the percent error (PE) in the mass estimate calculated as $(M_{\text{ST}} - M_{\text{true}})/M_{\text{true}} \times 100\%$. *Bottom:* residuals in Σ compared to the best-fit ST model.

Overall, this suggests that errors in the convergence and shear profiles are dominated by assumptions of the initial profile rather than the tidal mass-loss model; i.e., while an ST model does a fairly good job of predicting the convergence and shear of subhalo profiles, different values of the Einasto α value can introduce larger differences. Thus, we suspect that using updated tidal models (such as the Energy Truncation model) is unlikely to improve models of satellite lensing.

Previous work typically finds that different lens models introduce an error of ~ 10 per cent in mass estimates [e.g. 3, 57, 73]. Additionally, it has been found that even strong tidal truncation has a negligible effect on fitted subhalo parameters [M_{200} and concentration; 59] — however, M_{200} is not necessarily a good estimation of the bound subhalo mass. We explore the effect of profile assumptions on subhalo mass estimates in Figure 15. We assume that all projected density profiles can be well-described by a sharp truncation of the NFW model (i.e. the ST model), and fit the free parameters r_s , ρ_0 , and r_t . We then calculated the total mass by integrating the projected density profile. We find that the relative error in the subhalo mass typically ranges from 5–10 per cent.

5.2 Model Sensitivity in Lensing: Summary

We find that while there is a significant (30% or more) difference in the projected density and shear between NFW and Einasto profiles with different values of α , the tidal stripping model is less important. The central values of lensing observables predicted by the Energy Truncation model are within $\sim 10\%$ of those predicted by the ST (sharp truncation) approximation. In

particular, subhalo mass estimates based on ST are accurate to within 10 per cent, regardless of the mass profile assumed. Thus, for lensing applications, modelling results are not sensitive to assumptions about tidal stripping models.

6 Discussion

In this work, we have considered the implications of the uncertainty in subhalo density profiles and tidal evolution for calculations of the dark matter annihilation rate and lensing signals. Overall, we find that the annihilation rate and boost factor are very sensitive to both the subhalo profile and mass loss modelling; at small bound mass ratios, different assumptions lead to annihilation signals that differ by an order of magnitude. While there were also varying predictions in the quantities measured in subhalo lensing, we find that these are generally much less sensitive.

As discussed in [26, 27], since subhalo evolution is primarily understood from idealized simulations (due to resolution constraints), predictions for subhalo evolution depend sensitively on the initial halo models assumed in simulations. Here, we have considered Einasto profiles spanning the range of α values one might expect to exist, and also NFW profiles, which are useful for comparison with earlier work. Since lower Einasto α values correspond to steeper density profiles, the results in this paper from the EinLow model are the most relevant for the case of microhaloes, the smallest structures to form in the early universe, whose size is determined by the free-streaming scale of the dark matter particles (although the peak-height dependence of the Einasto shape parameter complicates this statement slightly).

Assuming dark matter particles have a mass of 100 GeV, the mass of the smallest microhaloes is approximately Earth mass [e.g. 22]. It is expected that the central density profile of these microhaloes is steeper than that found in larger haloes and thus may contribute greatly to the dark matter annihilation signal [e.g. 79]. We found the concentration of EinLowT profiles increases rapidly during tidal stripping and has larger annihilation signals than NFWT profiles at a fixed mass. Interestingly, in [29], it was found that Einasto profiles with low α values were the only ones that decreased in concentration after *major* mergers. These results all suggest that profiles with cuspiest centres (as found in the earliest haloes) evolve differently.

[45] found that microhaloes may have much higher densities than expected from extrapolations of the low-redshift concentration–mass–redshift relations, and [68] showed that if these densities are conserved, concentrations of the smallest haloes are still uncertain by a factor of ~ 5 when extrapolated to low redshift (considering the redshift evolution of the virial radius). [68] show that this uncertainty in concentration translates to an increased boost factor by up to two orders of magnitude. In our work, we find that the Energy Truncation model results in boost factors that are approximately 5 times higher at a given effective concentration (Figure 9). These results offer separate evidence that the boost factors of the smallest haloes may be greatly underestimated.

While we have focused on dark matter annihilation and lensing applications, subhaloes can also be used to study the nature of dark matter through stellar streams created by disrupted dwarf galaxies. For example, stream morphology can help constrain the potential of the host dark matter halo [e.g. 12], and features in streams caused by perturbations from other subhaloes can be used to place constraints on dark matter properties [e.g. 8]. In particular, there has been a lot of interest in studying the GD–1 stellar stream [6], which may have been perturbed by a compact dark matter subhalo. Other applications include semi-analytic models of galaxy formation, of which subhalo evolution models are often a key component

[e.g. 47, 90]. We leave the implications of conserved central density on these applications to future work.

A major assumption in this work is that the Energy Truncation model is an accurate representation of subhalo evolution. However, this model has several assumptions that are important to address. First, the infalling subhaloes are assumed to be spherical and isotropic. We expect that as the material is stripped off of subhaloes, the subhalo quickly becomes spherical and isotropic [26], and therefore this assumption is approximately valid. However, we plan to explore tidal stripping on non-spherical systems in future work. One way to create non-spherical initial conditions for idealized simulations is by using the output of major merger simulations, as proposed in [60]; in future work, we plan to use the simulations presented in [28, 29] to explore stripping of non-spherical systems.

Perhaps the most important assumption made in the Energy Truncation model is that subhaloes only evolve due to tidal fields, and there is no interaction with a baryonic component; extensive work has shown that baryonic matter influences dwarf galaxy properties [as reviewed in 7]. It has been proposed that dwarf galaxy haloes can transform from cusps to cores based on the stellar-to-halo mass ratio, M_*/M_{200} [70], where the cusp is protected from supernova feedback if $M_*/M_{200} \lesssim 5 \times 10^{-4}$ [21], which has been supported by several measurements [13, 72]. These considerations may be relevant for weak lensing studies of substructure since they centre on subhaloes with associated stellar mass by definition. For annihilation studies, on mass scales of $M_{200} < 10^{10} M_\odot$ below the dwarf galaxy range, star formation should be greatly suppressed by photo-heating [e.g. 41, 66]. Therefore, it is expected that dark-matter-dominated systems (down to putative Earth-mass-sized haloes) should not be affected by baryonic feedback. These dark matter-dominated systems may contribute greatly to an annihilation signal.

Finally, this work has focused on the effect of subhalo structure on the annihilation signal from individual haloes. To understand what this means, for a complex system like the Milky Way, we would need to model a full population of subhaloes, merging at different times on different orbits and with different concentration parameters. Estimating the signal directly in a self-consistent simulation requires properly correcting for numerical mass loss, which in turn is sensitive to the tidal stripping model assumed. In this paper we have included an initial analysis of the implications for measured dark matter annihilation in the Milky Way. In future work, we plan to track subhalo evolution in a cosmological simulation, using the Energy Truncation model to correct for artificial disruption. We will then use this corrected population to determine the total annihilation rate and place new constraints on proposed dark matter annihilation signals.

7 Conclusion

Our best hope for constraining the properties of dark matter through astrophysical observations comes from tests at the highest dark matter densities. Important examples include searches for a gamma-ray or other signal from dark matter annihilation, and tests of substructure in gravitational lenses. The inferences derived from observations depend strongly on the assumed clustering of dark matter on the smallest scales. Unfortunately, this remains unclear from theory; while there has been progress in understanding the average density profile of isolated haloes, including the smallest ones, it remains unclear how this profile evolves once these become subhaloes. Idealized cases of single mergers have been simulated at increasing resolution, but remain susceptible to numerical effects which can cause increased mass loss

[e.g. 82, 83] and decreased central densities [e.g. 27, 33]. To attempt to overcome numerical limitations, we have used a theoretically motivated, universal Energy Truncation method to study subhalo evolution. We quantify the effect of underestimating the central density of tidally-stripped haloes on annihilation signals and lensing profiles of individual subhaloes.

For lensing mass experiments, we conclude that the details of tidal stripping are less important than assumptions about the original density profile. Thus, recent estimates of the uncertainties in mass introduced by different profiles (approximately 10 per cent) are likely reliable. On the other hand, annihilation constraints are extremely sensitive to uncertainties both in subhalo profiles and in the details of tidal stripping. In particular, our Energy Truncation method predicts annihilation signals that are an order of magnitude larger than some previous estimates. Our initial calculations indicate that the total Milky Way annihilation signal may differ by a factor of five or more depending on the subhalo model used; however, the full annihilation calculation is complicated, and beyond the scope of this paper. Future work needs to be done to fully quantify the uncertainties in current dark matter annihilation constraints in light of updated subhalo evolution models.

Acknowledgments

NED acknowledges support from NSERC Canada, through a postgraduate scholarship. JET acknowledges financial support from NSERC Canada, through a Discovery Grant.

Software: numpy [38], matplotlib [42], scipy [84], COLOSSUS [24].

References

- [1] Shin’ichiro Ando, Tomoaki Ishiyama, and Nagisa Hiroshima. Halo Substructure Boosts to the Signatures of Dark Matter Annihilation. *Galaxies*, 7(3):68, Jul 2019.
- [2] Raul E. Angulo, Oliver Hahn, Aaron D. Ludlow, and Silvia Bonoli. Earth-mass haloes and the emergence of NFW density profiles. *MNRAS*, 471(4):4687–4701, Nov 2017.
- [3] Edward A. Baltz, Phil Marshall, and Masamune Oguri. Analytic models of plausible gravitational lens potentials. *J. Cosmology Astropart. Phys.*, 2009(1):015, Jan 2009.
- [4] Richard Bartels and Shin’ichiro Ando. Boosting the annihilation boost: Tidal effects on dark matter subhalos and consistent luminosity modeling. *Phys. Rev. D*, 92(12):123508, Dec 2015.
- [5] Andrew J. Benson and Xiaolong Du. Tidal tracks and artificial disruption of cold dark matter haloes. *MNRAS*, 517(1):1398–1406, November 2022.
- [6] Ana Bonaca, Charlie Conroy, David W. Hogg, Phillip A. Cargile, Nelson Caldwell, Rohan P. Naidu, Adrian M. Price-Whelan, Joshua S. Speagle, and Benjamin D. Johnson. High-resolution Spectroscopy of the GD-1 Stellar Stream Localizes the Perturber near the Orbital Plane of Sagittarius. *ApJ*, 892(2):L37, April 2020.
- [7] James S. Bullock and Michael Boylan-Kolchin. Small-Scale Challenges to the Λ CDM Paradigm. *ARA&A*, 55(1):343–387, Aug 2017.
- [8] Raymond G. Carlberg. The Density Structure of Simulated Stellar Streams. *ApJ*, 889(2):107, February 2020.
- [9] Laura J. Chang and Lina Necib. Dark matter density profiles in dwarf galaxies: linking Jeans modelling systematics and observation. *MNRAS*, 507(4):4715–4733, November 2021.
- [10] J.-H. Choi, M. D. Weinberg, and N. Katz. The dynamics of satellite disruption in cold dark matter haloes. *MNRAS*, 400:1247–1263, December 2009.

- [11] Camila A. Correa, J. Stuart B. Wyithe, Joop Schaye, and Alan R. Duffy. The accretion history of dark matter haloes - III. A physical model for the concentration-mass relation. *MNRAS*, 452(2):1217–1232, September 2015.
- [12] Biwei Dai, Brant E. Robertson, and Piero Madau. Around the Way: Testing Λ CDM with Milky Way Stellar Stream Constraints. *ApJ*, 858(2):73, May 2018.
- [13] Michele De Leo, Justin I. Read, Noelia E. D. Noel, Denis Erkal, Pol Massana, and Ricardo Carrera. Surviving the Waves: evidence for a Dark Matter cusp in the tidally disrupting Small Magellanic Cloud. *arXiv e-prints*, page arXiv:2303.08838, March 2023.
- [14] M. Sten Delos. Tidal evolution of dark matter annihilation rates in subhalos. *Phys. Rev. D*, 100(6):063505, Sep 2019.
- [15] M. Sten Delos, Margie Bruff, and Adrienne L. Erickcek. Predicting the density profiles of the first halos. *Phys. Rev. D*, 100(2):023523, Jul 2019.
- [16] M. Sten Delos, Michael Korsmeier, Axel Widmark, Carlos Blanco, Tim Linden, and Simon D. M. White. Limits on dark matter annihilation in prompt cusps from the isotropic gamma-ray background. *arXiv e-prints*, page arXiv:2307.13023, July 2023.
- [17] M. Sten Delos, Tim Linden, and Adrienne L. Erickcek. Breaking a dark degeneracy: The gamma-ray signature of early matter domination. *Phys. Rev. D*, 100(12):123546, Dec 2019.
- [18] M. Sten Delos and Simon D. M. White. Prompt cusps and the dark matter annihilation signal. *arXiv e-prints*, page arXiv:2209.11237, September 2022.
- [19] M. Sten Delos and Simon D. M. White. Inner cusps of the first dark matter haloes: formation and survival in a cosmological context. *MNRAS*, 518(3):3509–3532, January 2023.
- [20] Giulia Despali, Carlo Giocoli, Raul E. Angulo, Giuseppe Tormen, Ravi K. Sheth, Giacomo Baso, and Lauro Moscardini. The universality of the virial halo mass function and models for non-universality of other halo definitions. *MNRAS*, 456(3):2486–2504, March 2016.
- [21] Arianna Di Cintio, Chris B. Brook, Andrea V. Macciò, Greg S. Stinson, Alexander Knebe, Aaron A. Dutton, and James Wadsley. The dependence of dark matter profiles on the stellar-to-halo mass ratio: a prediction for cusps versus cores. *MNRAS*, 437(1):415–423, January 2014.
- [22] Roberta Diamanti, Maria Eugenia Cabrera Catalan, and Shin’ichiro Ando. Dark matter protohalos in a nine parameter MSSM and implications for direct and indirect detection. *Phys. Rev. D*, 92(6):065029, Sep 2015.
- [23] J. Diemand, M. Kuhlen, and P. Madau. Dark Matter Substructure and Gamma-Ray Annihilation in the Milky Way Halo. *ApJ*, 657:262–270, March 2007.
- [24] Benedikt Diemer. COLOSSUS: A Python Toolkit for Cosmology, Large-scale Structure, and Dark Matter Halos. *ApJS*, 239(2):35, December 2018.
- [25] N. E. Drakos, J. E. Taylor, and A. J. Benson. The phase-space structure of tidally stripped haloes. *MNRAS*, 468:2345–2358, June 2017.
- [26] Nicole E. Drakos, James E. Taylor, and Andrew J. Benson. Mass loss in tidally stripped systems; the energy-based truncation method. *MNRAS*, 494(1):378–395, May 2020.
- [27] Nicole E. Drakos, James E. Taylor, and Andrew J. Benson. A universal model for the evolution of tidally stripped systems. *MNRAS*, 516(1):106–123, October 2022.
- [28] Nicole E. Drakos, James E. Taylor, Anael Berrouet, Aaron S. G. Robotham, and Chris Power. Major mergers between dark matter haloes - I. Predictions for size, shape, and spin. *MNRAS*, 487(1):993–1007, Jul 2019.

- [29] Nicole E. Drakos, James E. Taylor, Anael Berrouet, Aaron S. G. Robotham, and Chris Power. Major mergers between dark matter haloes - II. Profile and concentration changes. *MNRAS*, 487(1):1008–1024, Jul 2019.
- [30] Andrej Dvornik, Henk Hoekstra, Konrad Kuijken, Angus H. Wright, Marika Asgari, Maciej Bilicki, Thomas Erben, Benjamin Giblin, Alister W. Graham, Catherine Heymans, Hendrik Hildebrandt, Andrew M. Hopkins, Arun Kannawadi, Chieh-An Lin, Edward N. Taylor, and Tilman Tröster. KiDS+GAMA: The weak lensing calibrated stellar-to-halo mass relation of central and satellite galaxies. *A&A*, 642:A83, October 2020.
- [31] A. S. Eddington. The distribution of stars in globular clusters. *MNRAS*, 76:572–585, May 1916.
- [32] J. Einasto. Kinematics and dynamics of stellar systems. *Trudy Inst. Astrofiz. Alma-Ata*, 5:87, 1965.
- [33] Raphaël Errani and Jorge Peñarrubia. Can tides disrupt cold dark matter subhaloes? *MNRAS*, 491(4):4591–4601, February 2020.
- [34] Gaétan Facchinetti, Julien Lavalle, and Martin Stref. Statistics for dark matter subhalo searches in gamma rays from a kinematically constrained population model: Fermi-LAT-like telescopes. *Phys. Rev. D*, 106(8):083023, October 2022.
- [35] L. Gao, J. F. Navarro, S. Cole, C. S. Frenk, S. D. M. White, V. Springel, A. Jenkins, and A. F. Neto. The redshift dependence of the structure of massive Λ cold dark matter haloes. *MNRAS*, 387:536–544, June 2008.
- [36] Sheridan B. Green and Frank C. van den Bosch. The tidal evolution of dark matter substructure - I. subhalo density profiles. *MNRAS*, 490(2):2091–2101, Dec 2019.
- [37] J. Han, S. Cole, C. S. Frenk, and Y. Jing. A unified model for the spatial and mass distribution of subhaloes. *MNRAS*, 457:1208–1223, April 2016.
- [38] Charles R. Harris, K. Jarrod Millman, Stéfan J. van der Walt, Ralf Gommers, Pauli Virtanen, David Cournapeau, Eric Wieser, Julian Taylor, Sebastian Berg, Nathaniel J. Smith, Robert Kern, Matti Picus, Stephan Hoyer, Marten H. van Kerkwijk, Matthew Brett, Allan Haldane, Jaime Fernández del Río, Mark Wiebe, Pearu Peterson, Pierre Gérard-Marchant, Kevin Sheppard, Tyler Reddy, Warren Weckesser, Hameer Abbasi, Christoph Gohlke, and Travis E. Oliphant. Array programming with NumPy. *Nature*, 585(7825):357–362, September 2020.
- [39] E. Hayashi, J. F. Navarro, J. E. Taylor, J. Stadel, and T. Quinn. The Structural Evolution of Substructure. *ApJ*, 584:541–558, February 2003.
- [40] Nagisa Hiroshima, Shin’ichiro Ando, and Tomoaki Ishiyama. Modeling evolution of dark matter substructure and annihilation boost. *Phys. Rev. D*, 97(12):123002, June 2018.
- [41] Matthias Hoeft, Gustavo Yepes, Stefan Gottlöber, and Volker Springel. Dwarf galaxies in voids: suppressing star formation with photoheating. *MNRAS*, 371(1):401–414, September 2006.
- [42] J. D. Hunter. Matplotlib: A 2d graphics environment. *Computing in Science & Engineering*, 9(3):90–95, 2007.
- [43] Moritz Hütten, Martin Stref, Céline Combet, Julien Lavalle, and David Maurin. γ -ray and ν Searches for Dark-Matter Subhalos in the Milky Way with a Baryonic Potential. *Galaxies*, 7(2):60, May 2019.
- [44] Alejandro Ibarra, Bradley J. Kavanagh, and Andreas Rappelt. Impact of substructure on local dark matter searches. *J. Cosmology Astropart. Phys.*, 2019(12):013, Dec 2019.
- [45] T. Ishiyama. Hierarchical Formation of Dark Matter Halos and the Free Streaming Scale. *ApJ*, 788:27, June 2014.
- [46] Tomoaki Ishiyama, Francisco Prada, Anatoly A. Klypin, Manodeep Sinha, R. Benton Metcalf, Eric Jullo, Bruno Altieri, Sofia A. Cora, Darren Croton, Sylvain de la Torre, David E.

- Millán-Calero, Taira Oogi, José Ruedas, and Cristian A. Vega-Martínez. The Uchuu simulations: Data Release 1 and dark matter halo concentrations. *MNRAS*, 506(3):4210–4231, September 2021.
- [47] Fangzhou Jiang, Avishai Dekel, Jonathan Freundlich, Frank C. van den Bosch, Sheridan B. Green, Philip F. Hopkins, Andrew Benson, and Xiaolong Du. SatGen: a semi-analytical satellite galaxy generator - I. The model and its application to Local-Group satellite statistics. *MNRAS*, 502(1):621–641, March 2021.
- [48] Fangzhou Jiang and Frank C. van den Bosch. Statistics of Dark Matter Substructure: I. Model and Universal Fitting Functions. *arXiv e-prints*, page arXiv:1403.6827, March 2014.
- [49] S. Kazantzidis, J. Magorrian, and B. Moore. Generating Equilibrium Dark Matter Halos: Inadequacies of the Local Maxwellian Approximation. *ApJ*, 601:37–46, January 2004.
- [50] Stelios Kazantzidis, Andrew R. Zentner, and Andrey V. Kravtsov. The Robustness of Dark Matter Density Profiles in Dissipationless Mergers. *ApJ*, 641(2):647–664, Apr 2006.
- [51] I. R. King. The structure of star clusters. III. Some simple dynamical models. *AJ*, 71:64, February 1966.
- [52] A. Klypin, G. Yepes, S. Gottlöber, F. Prada, and S. Heß. MultiDark simulations: the story of dark matter halo concentrations and density profiles. *MNRAS*, 457:4340–4359, April 2016.
- [53] Andrey V. Kravtsov. The Size-Virial Radius Relation of Galaxies. *ApJ*, 764(2):L31, February 2013.
- [54] Amit Kumar, Surhud More, and Divya Rana. Subaru HSC weak lensing of SDSS redMaPPer cluster satellite galaxies: empirical upper limit on orphan fractions. *MNRAS*, 517(3):4389–4404, December 2022.
- [55] Alexandres Lazar, James S. Bullock, Michael Boylan-Kolchin, Leonidas Moustakas, and Anna Nierenberg. An analytic surface density profile for Λ CDM halos and gravitational lensing studies. *arXiv e-prints*, page arXiv:2304.11177, April 2023.
- [56] Ran Li, Huanyuan Shan, Jean-Paul Kneib, Houjun Mo, Eduardo Rozo, Alexie Leauthaud, John Moustakas, Lizhi Xie, Thomas Erben, Ludovic Van Waerbeke, Martin Makler, Eli Rykoff, and Bruno Moraes. Measuring subhalo mass in redMaPPer clusters with CFHT Stripe 82 Survey. *MNRAS*, 458(3):2573–2583, May 2016.
- [57] Marceau Limousin, Jean-Paul Kneib, and Priyamvada Natarajan. Constraining the mass distribution of galaxies using galaxy-galaxy lensing in clusters and in the field. *MNRAS*, 356(1):309–322, Jan 2005.
- [58] Aaron D. Ludlow, Julio F. Navarro, Raúl E. Angulo, Michael Boylan-Kolchin, Volker Springel, Carlos Frenk, and Simon D. M. White. The mass-concentration-redshift relation of cold dark matter haloes. *MNRAS*, 441(1):378–388, June 2014.
- [59] Quinn Minor, Manoj Kaplinghat, Tony H. Chan, and Emily Simon. Inferring the concentration of dark matter subhaloes perturbing strongly lensed images. *MNRAS*, 507(1):1202–1215, October 2021.
- [60] B. Moore, S. Kazantzidis, J. Diemand, and J. Stadel. The origin and tidal evolution of cuspy triaxial haloes. *MNRAS*, 354:522–528, October 2004.
- [61] Priyamvada Natarajan, Jean-Paul Kneib, and Ian Smail. Evidence for Tidal Stripping of Dark Matter Halos in Massive Cluster Lenses. *ApJ*, 580(1):L11–L15, Nov 2002.
- [62] J. F. Navarro, C. S. Frenk, and S. D. M. White. The Structure of Cold Dark Matter Halos. *ApJ*, 462:563, May 1996.
- [63] J. F. Navarro, C. S. Frenk, and S. D. M. White. A Universal Density Profile from Hierarchical Clustering. *ApJ*, 490:493–508, December 1997.

- [64] J. F. Navarro, E. Hayashi, C. Power, A. R. Jenkins, C. S. Frenk, S. D. M. White, V. Springel, J. Stadel, and T. R. Quinn. The inner structure of Λ CDM haloes - III. Universality and asymptotic slopes. *MNRAS*, 349:1039–1051, April 2004.
- [65] Anna Niemiec, Eric Jullo, Marceau Limousin, Carlo Giocoli, Thomas Erben, Hendrik Hildebrandt, Jean-Paul Kneib, Alexie Leauthaud, Martin Makler, Bruno Moraes, Maria E. S. Pereira, Huanyuan Shan, Eduardo Rozo, Eli Rykoff, and Ludovic Van Waerbeke. Stellar-to-halo mass relation of cluster galaxies. *MNRAS*, 471(1):1153–1166, October 2017.
- [66] Yookyung Noh and Matthew McQuinn. A physical understanding of how reionization suppresses accretion on to dwarf haloes. *MNRAS*, 444(1):503–514, October 2014.
- [67] Go Ogiya and Oliver Hahn. What sets the central structure of dark matter haloes? *MNRAS*, 473(4):4339–4359, Feb 2018.
- [68] C. Okoli, J. E. Taylor, and N. Afshordi. Searching for dark matter annihilation from individual halos: uncertainties, scatter and signal-to-noise ratios. *J. Cosmology Astropart. Phys.*, 8:019, August 2018.
- [69] J. Peñarrubia, A. J. Benson, M. G. Walker, G. Gilmore, A. W. McConnachie, and L. Mayer. The impact of dark matter cusps and cores on the satellite galaxy population around spiral galaxies. *MNRAS*, 406:1290–1305, August 2010.
- [70] Jorge Peñarrubia, Andrew Pontzen, Matthew G. Walker, and Sergey E. Kroupov. The Coupling between the Core/Cusp and Missing Satellite Problems. *ApJ*, 759(2):L42, November 2012.
- [71] Planck Collaboration, N. Aghanim, Y. Akrami, M. Ashdown, J. Aumont, C. Baccigalupi, M. Ballardini, A. J. Banday, R. B. Barreiro, N. Bartolo, S. Basak, R. Battye, K. Benabed, J. P. Bernard, M. Bersanelli, P. Bielewicz, J. J. Bock, J. R. Bond, J. Borrill, F. R. Bouchet, F. Boulanger, M. Bucher, C. Burigana, R. C. Butler, E. Calabrese, J. F. Cardoso, J. Carron, A. Challinor, H. C. Chiang, J. Chluba, L. P. L. Colombo, C. Combet, D. Contreras, B. P. Crill, F. Cuttaia, P. de Bernardis, G. de Zotti, J. Delabrouille, J. M. Delouis, E. Di Valentino, J. M. Diego, O. Doré, M. Douspis, A. Ducout, X. Dupac, S. Dusini, G. Efstathiou, F. Elsner, T. A. Enßlin, H. K. Eriksen, Y. Fantaye, M. Farhang, J. Fergusson, R. Fernandez-Cobos, F. Finelli, F. Forastieri, M. Frailis, A. A. Fraisse, E. Franceschi, A. Frolov, S. Galeotta, S. Galli, K. Ganga, R. T. Génova-Santos, M. Gerbino, T. Ghosh, J. González-Nuevo, K. M. Górski, S. Gratton, A. Gruppuso, J. E. Gudmundsson, J. Hamann, W. Handley, F. K. Hansen, D. Herranz, S. R. Hildebrandt, E. Hivon, Z. Huang, A. H. Jaffe, W. C. Jones, A. Karakci, E. Keihänen, R. Kesitalo, K. Kiiveri, J. Kim, T. S. Kisner, L. Knox, N. Krachmalnicoff, M. Kunz, H. Kurki-Suonio, G. Lagache, J. M. Lamarre, A. Lasenby, M. Lattanzi, C. R. Lawrence, M. Le Jeune, P. Lemos, J. Lesgourgues, F. Levrier, A. Lewis, M. Liguori, P. B. Lilje, M. Lilley, V. Lindholm, M. López-Cañiego, P. M. Lubin, Y. Z. Ma, J. F. Macías-Pérez, G. Maggio, D. Maino, N. Mandolesi, A. Mangilli, A. Marcos-Caballero, M. Maris, P. G. Martin, M. Martinelli, E. Martínez-González, S. Matarrese, N. Mauri, J. D. McEwen, P. R. Meinhold, A. Melchiorri, A. Mennella, M. Migliaccio, M. Millea, S. Mitra, M. A. Miville-Deschênes, D. Molinari, L. Montier, G. Morgante, A. Moss, P. Natoli, H. U. Nørgaard-Nielsen, L. Pagano, D. Paoletti, B. Partridge, G. Patanchon, H. V. Peiris, F. Perrotta, V. Pettorino, F. Piacentini, L. Polastri, G. Polenta, J. L. Puget, J. P. Rachen, M. Reinecke, M. Remazeilles, A. Renzi, G. Rocha, C. Rosset, G. Roudier, J. A. Rubiño-Martín, B. Ruiz-Granados, L. Salvati, M. Sandri, M. Savelainen, D. Scott, E. P. S. Shellard, C. Sirignano, G. Sirri, L. D. Spencer, R. Sunyaev, A. S. Suur-Uski, J. A. Tauber, D. Tavagnacco, M. Tenti, L. Toffolatti, M. Tomasi, T. Trombetti, L. Valenziano, J. Valiviita, B. Van Tent, L. Vibert, P. Vielva, F. Villa, N. Vittorio, B. D. Wandelt, I. K. Wehus, M. White, S. D. M. White, A. Zacchei, and A. Zonca. Planck 2018 results. VI. Cosmological parameters. *arXiv e-prints*, page arXiv:1807.06209, July 2018.
- [72] J. I. Read, M. G. Walker, and P. Steger. Dark matter heats up in dwarf galaxies. *MNRAS*, 484(1):1401–1420, March 2019.

- [73] Mauro Sereno, Cosimo Fedeli, and Lauro Moscardini. Comparison of weak lensing by NFW and Einasto halos and systematic errors. *J. Cosmology Astropart. Phys.*, 2016(1):042, January 2016.
- [74] Cristóbal Sifón, Ricardo Herbonnet, Henk Hoekstra, Remco F. J. van der Burg, and Massimo Viola. The galaxy-subhalo connection in low-redshift galaxy clusters from weak gravitational lensing. *MNRAS*, 478(1):1244–1264, July 2018.
- [75] Rachel S. Somerville, Peter Behroozi, Viraj Pandya, Avishai Dekel, S. M. Faber, Adriano Fontana, Anton M. Koekemoer, David C. Koo, P. G. Pérez-González, Joel R. Primack, Paola Santini, Edward N. Taylor, and Arjen van der Wel. The relationship between galaxy and dark matter halo size from $z \sim 3$ to the present. *MNRAS*, 473(2):2714–2736, January 2018.
- [76] Martin Stref, Thomas Lacroix, and Julien Laval. Remnants of Galactic Subhalos and Their Impact on Indirect Dark-Matter Searches. *Galaxies*, 7(2):65, June 2019.
- [77] Martin Stref and Julien Laval. Modeling dark matter subhalos in a constrained galaxy: Global mass and boosted annihilation profiles. *Phys. Rev. D*, 95(6):063003, Mar 2017.
- [78] Jens Stücker, Raul E. Angulo, and Philipp Busch. The boosted potential. *MNRAS*, 508(4):5196–5216, December 2021.
- [79] Jens Stücker, Go Ogiya, Simon D. M. White, and Raul E. Angulo. The effect of stellar encounters on the dark matter annihilation signal from prompt cusps. *MNRAS*, 523(1):1067–1088, July 2023.
- [80] J. E. Taylor and J. Silk. The clumpiness of cold dark matter: implications for the annihilation signal. *MNRAS*, 339:505–514, February 2003.
- [81] James E. Taylor, Jihye Shin, Nathalie N. Q. Ouellette, and Stéphane Courteau. The assembly of the Virgo cluster, traced by its galaxy haloes. *MNRAS*, 488(1):1111–1126, September 2019.
- [82] F. C. van den Bosch and G. Ogiya. Dark matter substructure in numerical simulations: a tale of discreteness noise, runaway instabilities, and artificial disruption. *MNRAS*, 475:4066–4087, April 2018.
- [83] F. C. van den Bosch, G. Ogiya, O. Hahn, and A. Burkert. Disruption of dark matter substructure: fact or fiction? *MNRAS*, 474:3043–3066, March 2018.
- [84] Pauli Virtanen, Ralf Gommers, Travis E. Oliphant, Matt Haberland, Tyler Reddy, David Cournapeau, Evgeni Burovski, Pearu Peterson, Warren Weckesser, Jonathan Bright, Stéfan J. van der Walt, Matthew Brett, Joshua Wilson, K. Jarrod Millman, Nikolay Mayorov, Andrew R. J. Nelson, Eric Jones, Robert Kern, Eric Larson, C J Carey, İlhan Polat, Yu Feng, Eric W. Moore, Jake VanderPlas, Denis Laxalde, Josef Perktold, Robert Cimrman, Ian Henriksen, E. A. Quintero, Charles R. Harris, Anne M. Archibald, Antônio H. Ribeiro, Fabian Pedregosa, Paul van Mulbregt, and SciPy 1.0 Contributors. SciPy 1.0: Fundamental Algorithms for Scientific Computing in Python. *Nature Methods*, 17:261–272, 2020.
- [85] Chunxiang Wang, Ran Li, Huanyuan Shan, Weiwei Xu, Ji Yao, Yingjie Jing, Liang Gao, Nan Li, Yushan Xie, Kai Zhu, Hang Yang, and Qingze Chen. Assessing mass-loss and stellar-to-halo mass ratio of satellite galaxies: a galaxy-galaxy lensing approach utilizing DECaLS DR8 data. *MNRAS*, 528(2):2728–2741, February 2024.
- [86] Kuan Wang, Yao-Yuan Mao, Andrew R. Zentner, Johannes U. Lange, Frank C. van den Bosch, and Risa H. Wechsler. Concentrations of dark haloes emerge from their merger histories. *MNRAS*, 498(3):4450–4464, November 2020.
- [87] R. H. Wechsler, J. S. Bullock, J. R. Primack, A. V. Kravtsov, and A. Dekel. Concentrations of Dark Halos from Their Assembly Histories. *ApJ*, 568:52–70, March 2002.
- [88] L. M. Widrow and J. Dubinski. Equilibrium Disk-Bulge-Halo Models for the Milky Way and Andromeda Galaxies. *ApJ*, 631:838–855, October 2005.

- [89] A. W. C. Wong and J. E. Taylor. What Do Dark Matter Halo Properties Tell Us about Their Mass Assembly Histories? *ApJ*, 757:102, September 2012.
- [90] Shengqi Yang, Xiaolong Du, Andrew J. Benson, Anthony R. Pullen, and Annika H. G. Peter. A new calibration method of sub-halo orbital evolution for semi-analytic models. *MNRAS*, 498(3):3902–3913, November 2020.
- [91] D. H. Zhao, Y. P. Jing, H. J. Mo, and G. Börner. Accurate Universal Models for the Mass Accretion Histories and Concentrations of Dark Matter Halos. *ApJ*, 707:354–369, December 2009.
- [92] D. H. Zhao, H. J. Mo, Y. P. Jing, and G. Börner. The growth and structure of dark matter haloes. *MNRAS*, 339:12–24, February 2003.